
CONVERGENCE AND GENERALIZATION OF ANTI-REGULARIZATION FOR PARAMETRIC MODELS

Dongseok Kim, Wonjun Jeong, Gisung Oh

Department of Computer Engineering
Gachon University

Seongnam-si, Gyeonggi-do, South Korea
{jkds5920, tp04045, eustia}@gachon.ac.kr

ABSTRACT

We propose Anti-regularization (AR), which adds a sign-reversed reward term to the loss to intentionally increase model expressivity in the small-sample regime, and then attenuates this intervention with a power-law decay as the sample size grows. We formalize spectral safety and trust-region conditions, and design a lightweight stability safeguard that combines a projection operator with gradient clipping, ensuring stable intervention under stated assumptions. Our analysis spans linear smoothers and the Neural Tangent Kernel (NTK) regime, providing practical guidance on selecting the decay exponent by balancing empirical risk against variance. Empirically, AR reduces underfitting while preserving generalization and improving calibration in both regression and classification. Ablation studies confirm that the decay schedule and the stability safeguard are critical to preventing overfitting and numerical instability. We further examine a degrees-of-freedom targeting schedule that keeps per-sample complexity approximately constant. AR is simple to implement and reproducible, integrating cleanly into standard empirical risk minimization pipelines. It enables robust learning in data- and resource-constrained settings by intervening only when beneficial and fading away when unnecessary.

Keywords Convergence · Generalization · Regularization · Stability · Underfitting

1 Introduction

1.1 Motivation

While the adoption of artificial intelligence (AI) in industry has become widespread, small- and medium-sized enterprises (SMEs) and startups often begin with limited samples due to constraints in computing resources and data infrastructure. These disparities and practical limitations have been repeatedly highlighted in international comparisons. According to OECD reports [1, 2], there are pronounced gaps in AI adoption and capabilities across industries, regions, and firm sizes. In particular, SMEs suffer from structural bottlenecks in data acquisition, quality control, and operational deployment in early-stage AI projects, due to limited computing resources, poor data governance, and insufficient talent capacity. These realities suggest the need for a training procedure that delivers immediately usable performance while avoiding underfitting, especially under the assumption that real-world applications often begin with small samples.

In data-scarce environments, acquiring additional samples can be prohibitively costly and time-consuming. Privacy regulations and industry norms also hinder data sharing and integration. The European Parliamentary Research Service [3] notes that GDPR imposes constraints on AI training data through the principles of data minimization and purpose limitation. In practice, small-sample learning scenarios are common. Tian et al. [4] systematize methodologies for incremental data settings, and Tao et al. [5] emphasize the intrinsic scarcity of samples in rare-event tasks such as industrial defect detection. While data augmentation is an important tool, it is not a panacea. Wang et al. [6] summarize both the benefits and limitations of augmentation, while Geirhos et al. [7] and Brown et al. [8] show how spurious correlations and shortcut learning can hinder generalization in real-world deployments.

In such early stages—where data is limited and risks of noise and bias coexist—traditional regularization, which suppresses model complexity, may exacerbate underfitting. Hastie et al. [9] review the bias–variance tradeoff and the impact of regularization in small-sample regimes, and Belkin et al. [10] demonstrate that expanding expressivity or relaxing constraints can, under certain conditions, improve generalization. In practice, the initial model performance—what is immediately available—often determines subsequent investment decisions and project continuation. Paleyes et al. [11] and Sculley et al. [12] highlight the criticality of early-stage performance validation, considering deployment constraints, technical debt, and cost structures.

This study aims to address such practical demands by proposing a training strategy that secures usable performance even in small-sample regimes, while enabling a stable transition to the final model without changing the architecture as data accumulates. Unlike continual learning, we perform retraining at each stage, adjusting the learning strategy according to the sample size to manage the overall training trajectory in a continuous manner. The conceptual distinction from continual learning can be referenced in De Lange et al. [13]. Since reversing the sign of a regularization term carries risks of divergence, we design safety mechanisms to ensure stable reward operation: spectral safety conditions for regression and trust-region constraints with bounded margin rewards for classification. Schulman et al. [14] and Cortes and Vapnik [15] offer the standard frameworks for trust-region constraints and margin-based design, respectively. The reward strength λ follows a decay schedule that gradually diminishes with the sample size n , so that as data accumulates, the effect of the reward naturally vanishes, ultimately converging to training without a regularization term.

1.2 Contributions

This study proposes Anti-regularization (AR), which adds a reward term to the loss function, to achieve immediately usable performance even in small-data and resource-constrained environments. The proposed method selectively enhances expressivity in the early stages to mitigate underfitting and gradually attenuates the reward strength as the sample size increases, enabling a smooth transition to a final model without regularization. The main contributions are as follows:

- **Theoretical formalization and safety conditions of Anti-regularization:** We formalize Anti-regularization, which introduces a reward term with a reversed sign into the loss, and establish design principles that prevent divergence in both regression and classification tasks. We also discuss its extensibility to shallow neural networks and the Neural Tangent Kernel regime.
- **Sample-size-dependent schedules and DoF targeting:** We propose a simple schedule that gradually reduces the reward strength with increasing sample size, and present an alternative degrees of freedom-based rule that maintains constant per-sample complexity.
- **Practical diagnostics for alleviating underfitting:** We outline a procedure to determine when to activate or deactivate Anti-regularization based on the joint trends of training error and model complexity, and provide monitoring metrics to verify its contribution to actual performance improvement.
- **Safe training protocol for classification tasks:** To avoid instability due to the absence of lower bounds, we construct a robust training procedure that combines trust-region constraints, bounded margin rewards, logits, and gradient clipping.
- **Lightweight and compatible implementation:** Targeting linear models and shallow multilayer perceptrons, we propose a practical protocol that boosts initial performance by adjusting only the loss function without modifying model architecture or hardware, then naturally transitions to a no-regularization model as data accumulates.
- **Systematic experiments for theoretical validation:** Focusing on tabular regression and image classification, we evaluate the validity, safety, and sensitivity of the proposed method and empirically verify its effectiveness through comparisons with alternative strategies.
- **Practical alternative for small organizations:** By securing reasonable initial performance without requiring high-performance computing or large-scale datasets, and by providing a transition path within a fixed model structure as data grows, we lower the barriers to AI adoption for SMEs and startups.

1.3 Paradigm Shifts in Regularization

Zhang et al. [16] challenged classical intuitions on generalization by showing that large neural networks can perfectly fit randomly labeled data without explicit regularization, while still achieving non-trivial generalization. Soudry et al. [17] proved that gradient descent implicitly converges to the maximum-margin separator in linearly separable settings, revealing that the learning algorithm itself can induce a strong implicit regularization effect. Bartlett et al. [18]

formalized the phenomenon of benign overfitting, where interpolating solutions in high-dimensional linear regression can still achieve test risk close to the noise level.

Belkin et al. [10] introduced the double descent curve, showing that as model capacity increases, test risk can decrease again after passing through the traditional U-shaped bias–variance tradeoff curve, highlighting a structural shift in generalization behavior around the interpolation threshold. Loog et al. [19] revisited literature from statistics and pattern recognition in the 1980s–1990s, showing that double descent phenomena had been previously observed and that modern results lie on a historical continuum rather than being an abrupt shift. Nakkiran et al. [20] systematically studied deep double descent along axes such as model width, training epochs, and data size. Adlam et al. [21] emphasized that a fine-grained bias–variance decomposition is key to understanding the underlying mechanism of double descent.

Hastie et al. [22] provided a rigorous risk analysis of ridgeless minimum-norm interpolators, showing that such solutions can generalize surprisingly well in overparameterized regimes. Belkin et al. [23] used two models to demonstrate how double descent arises under weak feature conditions. Muthukumar et al. [24] derived the harmless interpolation condition, showing that interpolation may not harm generalization when noise is spread across many less relevant directions.

Geiger et al. [25] proposed a jamming transition between under- and overparameterized regimes, explaining the spike in generalization error near the interpolation threshold and its subsequent decline using insights from loss landscape geometry. Spigler et al. [26] independently observed and analyzed similar transitions and generalization patterns, reinforcing their reproducibility. Advani et al. [27] used high-dimensional mean-field theory to quantify how the data-to-model ratio and signal-to-noise ratio mediate such transitions. Meanwhile, Nakkiran et al. [28] theoretically and empirically showed that the choice and strength of optimal (especially ℓ_2) regularization can mitigate double descent, suggesting that regularization should be contextually designed rather than uniformly strong.

1.4 Anti-regularization and Reward-Based Objectives

Unlike traditional regularization, which suppresses model complexity by adding penalties to the loss function, reward-based objectives—adding terms that promote specific behaviors or properties—have been explored across various contexts. Pereyra et al. [29] introduced a confidence penalty to reduce overconfident predictions, and Szegedy et al. [30] used label smoothing to soften the target distribution and suppress excessive certainty. Müller et al. [31] systematically analyzed the effects of smoothing, highlighting its benefits in terms of generalization and uncertainty calibration. Kim et al. [32] proposed negative learning, which uses incorrect labels as learning signals to enhance robustness in noisy-label settings, while Ishida et al. [33] restructured the objective to rely on complementary labels instead of correct ones.

In sequence learning, efforts have been made to directly optimize task-specific rewards. Ranzato et al. [34] proposed learning sequence-level rewards using REINFORCE, and Norouzi et al. [35] generalized maximum likelihood training into reward-aligned learning via reward-proportional distributions. In language model fine-tuning guided by human preferences, Christiano et al. [36] and Ziegler et al. [37] proposed policy improvement via reward models trained on human feedback, and Ouyang et al. [38] demonstrated their effectiveness in large-scale instruction-following. More recently, Rafailov et al. [39] proposed a supervised alternative that implicitly maximizes rewards from preference data without explicit reinforcement learning.

In representation learning, contrastive learning adopts a reward structure that promotes similarity among positive pairs and separation among negative pairs. van den Oord et al. [40] proposed a contrastive loss that maximizes a lower bound on mutual information, encouraging high-information representations. On the other hand, adversarial objectives designed to eliminate unwanted factors are closer to anti-reward mechanisms. Ganin et al. [41] used gradient reversal to make the domain classification loss act in reverse, preventing domain information from being encoded. Zhang et al. [42] trained with an adversary to remove bias signals by targeting sensitive attribute predictors. In reinforcement learning, Haarnoja et al. [43] incorporated entropy rewards into the reward function, formalizing the maximum entropy objective to enhance exploration and robustness.

1.5 Sample-Size-Dependent Regularization and Degrees of Freedom Control

The classical idea of adjusting regularization strength based on sample size and targeting a desired level of effective degrees of freedom has been established in information criteria, risk estimation, and cross-validation theory. Akaike [44] penalized model complexity (number of effective parameters) as a constant term in the AIC, correcting bias in generalization error. Mallows [45] introduced the C_p criterion as an unbiased estimate of prediction error. Stein [46] enabled data-adaptive shrinkage via Stein’s Unbiased Risk Estimate (SURE), and Craven et al. [47] formalized generalized cross-validation (GCV) for choosing smoothing parameters in a data-dependent manner. Wahba [48] established the equivalence between degrees of freedom and smoothness control in spline regularization. Ye [49] defined

generalized degrees of freedom (GDF) as the sum of sensitivities of fitted values to observations and showed that, in linear smoothers, it matches the trace of the hat matrix—providing a theoretical foundation for data-driven complexity penalties. Hastie et al. [9] unified these criteria from a common perspective and discussed practical rules for gradually relaxing penalties as the sample size increases to avoid underfitting and minimize prediction risk.

In sparsity-inducing regularization, the interplay between degrees of freedom and penalty strength has also been rigorously analyzed. Efron et al. [50] described the piecewise linear structure of the Lasso path and how degrees of freedom vary along it. Zou et al. [51] showed that the degrees of freedom of the Lasso can be approximated by the number of active variables under general conditions. Tibshirani et al. [52] characterized the degrees of freedom of Lasso-type problems under convexity and regularity assumptions, providing quantitative guidance for scaling regularization with respect to sample size and signal strength. Donoho et al. [53] demonstrated that SURE-based threshold selection enables data-dependent shrinkage that minimizes risk, and Stone [54] theoretically justified cross-validation as a mechanism for balancing underfitting and overfitting as sample size increases.

At the level of training procedures, early stopping has been shown to act as a data-dependent form of regularization. Prechelt [55] empirically demonstrated that using validation error to define stopping criteria suppresses overfitting by providing a regularization effect. Yao et al. [56] showed that early stopping in gradient descent can be equivalent to Tikhonov regularization under certain conditions. Raskutti et al. [57] derived generalization bounds in nonparametric regression when the number of iterations is chosen based on sample size, supporting the conclusion that longer training or weaker explicit regularization becomes favorable as data grows.

In stochastic optimization, the noise scale induced by batch size and learning rate has been increasingly recognized as an implicit regularization mechanism, which must be co-scheduled with sample size. Mandt et al. [58] approximated SGD as a stochastic differential equation and showed that noise temperature plays a regularization role by mediating between prior and posterior. Smith et al. [59] explained optimal generalization using a scaling law between batch size, learning rate, and dataset size. Jastrzebski et al. [60] reported how combinations of data size, learning rate, and batch size influence flat minima and generalization. Keskar et al. [61] pointed out that large batches may weaken implicit regularization, leading to generalization gaps. Loshchilov et al. [62] decoupled weight decay from optimization steps to enable better scheduling, and Smith [63] proposed cyclical learning rates to dynamically control the strength of implicit regularization in practice.

1.6 Classification Safety and Training Stability

Safe training in classification tasks has been pursued through overconfidence mitigation, robustness to noise and perturbations, smooth decision boundaries, and algorithmic stability. Bousquet et al. [64] established that uniform stability provides generalization bounds, offering a theoretical foundation for safe objective functions and algorithm design. Hardt et al. [65] analyzed the data-dependent stability of SGD and formalized its relationship with learning rate, iteration count, and generalization. Guo et al. [66] highlighted the severe overconfidence problem in modern neural networks and demonstrated that temperature scaling can effectively calibrate predictions. Müller et al. [31] systematically showed that label smoothing improves both generalization and probabilistic calibration.

In label noise settings, loss redesign has been a key approach. Patrini et al. [67] proposed correcting the loss by estimating the noise transition matrix, while Ghosh et al. [68] theoretically analyzed the robustness of symmetric losses. Zhang et al. [69] introduced a generalized loss that interpolates between cross-entropy and MAE, achieving a balance between robustness and convergence. Wang et al. [70] added a symmetric term to standard cross-entropy to enhance stability under mislabeled data.

Methods that promote local smoothness and large margins help secure safe decision boundaries. Miyato et al. [71] enforced output invariance to small perturbations, ensuring local smoothness in classifiers. Zhang et al. [72] proposed mixup, which linearly interpolates both inputs and labels to smooth decision boundaries and reduce both overfitting and overconfidence. Thulasidasan et al. [73] showed that mixup is particularly effective for confidence calibration. Pascanu et al. [74] formalized that gradient clipping suppresses exploding updates and improves numerical stability during training. Loshchilov et al. [62] proposed AdamW to decouple weight decay from optimization steps, improving tuning and convergence stability.

Safety against adversarial perturbations has been approached through robust optimization and certification methods. Madry et al. [75] established a standard min-max training procedure for learning classifiers robust to ℓ_p perturbations. Zhang et al. [76] proposed TRADES, characterizing the fundamental trade-off between robustness and accuracy and providing generalization bounds. Cissé et al. [77] proposed controlling Lipschitz bounds at the layer level to suppress perturbation amplification, and Cohen et al. [78] provided certified robustness within an ℓ_2 radius via randomized smoothing.

1.7 NTK Extensions and Directional Regularization from Spectral and Kernel Perspectives

Jacot et al. [79] showed that as neural network width tends to infinity, the network linearizes into fixed kernel regression, with its learning dynamics governed by the Neural Tangent Kernel (NTK). Lee et al. [80] reinforced the generality of the NTK regime by proving that wide networks of arbitrary depth evolve like linear models under gradient descent. Chizat et al. [81] formalized the lazy training regime, where parameter changes remain small in the large-width limit, explaining kernel-like behavior when feature learning is limited. Du et al. [82] supported the optimization perspective of the NTK regime by proving that gradient descent converges to global minima under overparameterization.

The generalization of kernel regression has been shown to depend on the kernel eigenspectrum and task–model alignment. Bordelon et al. [83] quantified how learning curves vary with the kernel eigenspectrum and the target’s projection onto the kernel eigenfunctions. Canatar et al. [84] demonstrated that tasks aligned with the principal components of the kernel lead to higher sample efficiency, formalizing the alignment principle. Liang et al. [85] identified conditions under which interpolation without ridge regularization can still generalize, and Hastie et al. [22] analyzed the risk of high-dimensional minimum-norm interpolators, revealing the spectral dependence of kernel and linear solutions. Mei et al. [86] provided an exact high-dimensional characterization of the risk in random features regression, analyzing the spectral effects of kernel approximations.

From the kernel approximation viewpoint, Rahimi et al. [87] proposed random features as an efficient method for approximating kernels, and Rudi et al. [88] established generalization guarantees for such methods. Rahaman et al. [89] observed spectral bias in neural networks, showing that networks tend to learn functions from low to high frequencies, thereby linking neural network behavior to kernel and NTK-based analysis.

The classical framework for directional regularization has been established in Tikhonov regularization with weights and generalized ridge methods. Hoerl et al. [90] proposed shrinking along covariance directions to control estimation variance. Engl et al. [91] unified various regularization strategies—including Tikhonov and early stopping—under the spectral filtering perspective. Hansen [92] systematized how filter functions and penalty matrices can be used to selectively suppress or emphasize specific eigendirections.

2 Theoretical Analysis

This section aims to formalize AR as a reward term added to the empirical risk and to present the spectral safety condition and trust-region–based guarantees, the existence and convergence of solutions, conditions under which test error improves by correcting underfitting in small-sample regimes, the scaling rule for λ as a function of sample size n , classification-specific issues such as the lack of a lower bound and remedies via trust-region or bounded margin rewards, the extension to the NTK regime of shallow MLPs (1–3 layers), and a stability-oriented interpretation. Detailed proofs are provided in the appendix.

2.1 Notation and Symbols

To ensure clarity, the following set of notations is fixed throughout the paper. Key symbols are defined precisely and used consistently in subsequent theorems and proofs without redundancy. Eigenvalues are denoted by σ , and the regularization coefficient is denoted by λ to prevent notation conflicts.

- **Data and Model**

- Training set: $S = \{(x_i, y_i)\}_{i=1}^{|S|}$
- Parameters: θ , predictor: f_θ

- **Objective Function**

$$\hat{F}_\lambda(\theta) = \frac{1}{|S|} \sum_{(x,y) \in S} \ell(\theta; x, y) - \lambda R(\theta), \quad \lambda \geq 0$$

- **Loss Function**

- Regression: $\ell(\theta; x, y) = \frac{1}{2}(y - f_\theta(x))^2$
- Classification: $\ell(\theta; x, y) = H(p_y, q_\theta(x))$

- **Regularization Term**

- $R(\theta) = \frac{1}{2}\|\theta\|_2^2$
- or $R(\theta) = \frac{1}{2}\theta^\top W\theta$ (spectrally weighted)

- **Linear Regression Setup**
 - Design matrix: $X \in \mathbb{R}^{|S| \times p}$
 - Sample covariance: $\hat{\Sigma} = \frac{1}{|S|} X^\top X$
 - Eigenvalue notation: $\sigma_{\min}(\cdot)$, $\sigma_{\max}(\cdot)$
- **Linear Smoother and Degrees of Freedom**
 - Smoother: $S_\lambda = X(X^\top X - |S| \lambda I)^{-1} X^\top$
 - Degrees of freedom: $\text{tr}(S_\lambda)$
- **Noise Model**
 - $\varepsilon \sim (0, \tau^2 I)$
- **Classification-Specific Symbols**
 - Margin: $m_\theta(x, y)$
 - Bounded margin reward function: ϕ
 - Network Lipschitz constant: G
 - Margin threshold: γ
- **NTK**
 - Kernel: K

2.2 Safety (Existence and Convergence)

Theorem 1 (Spectral Safety Condition and Strong Convexity in Regression). *Let $\hat{\Sigma} = \frac{1}{|S|} X^\top X$ in linear regression. If $\lambda < \sigma_{\min}(\hat{\Sigma})$, then \hat{F}_λ is $\sigma_{\min}(\hat{\Sigma}) - \lambda$ strongly convex, and the global minimizer is unique.*

Proof Sketch. The Hessian is given by $\nabla^2 \hat{F}_\lambda = \hat{\Sigma} - \lambda I$. The smallest eigenvalue is $\sigma_{\min}(\hat{\Sigma}) - \lambda > 0$, which ensures strong convexity. \square

Corollary 2 (Closed-form Solution and Gradient Descent Stability). *The unique minimizer is given by $\hat{\theta}_\lambda = (X^\top X - |S| \lambda I)^{-1} X^\top y$. Moreover, if $0 < \eta < \frac{2}{\sigma_{\max}(\hat{\Sigma}) - \lambda}$, then gradient descent converges linearly.*

Lemma 3 (Lower Bound Guarantee in Classification). *In classification, the objective $H - \lambda \|\theta\|^2$ may be unbounded below on separable data. A minimizer exists if one of the following conditions holds. First, optimization is performed under a trust-region constraint $\|\theta\| \leq B$. Second, a bounded margin reward function ϕ is used, yielding:*

$$\hat{F}_\lambda(\theta) = \frac{1}{|S|} \sum H(p_y, q_\theta(x)) - \lambda \cdot \frac{1}{|S|} \sum \phi(m_\theta(x, y))$$

Proof Sketch. A trust-region constraint defines a compact domain, which ensures that the continuous objective admits a minimum. The bounded reward ϕ provides a lower bound for the objective. \square

2.3 Degrees of Freedom and Sample-size-Dependent Scaling (Regression)

The degrees of freedom of the linear smoother S_λ is given by $\text{tr}(S_\lambda) = \sum_{j=1}^p \frac{\sigma_j}{\sigma_j - \lambda}$, where $\{\sigma_j\}$ are the eigenvalues of $\hat{\Sigma}$. This quantity increases monotonically in λ within the spectral safety condition, and amplifies directions with smaller σ_j more strongly. Under the generative model $y = X\theta^* + \varepsilon$, the following optimism identity holds:

$$\mathbb{E}[\mathcal{R}(\hat{f}_\lambda)] = \mathbb{E}[\hat{\mathcal{R}}_S(\hat{f}_\lambda)] + \frac{2\tau^2}{|S|} \text{tr}(S_\lambda).$$

Theorem 4 (Condition for Correcting Underfitting). *Let $\Delta \hat{\mathcal{R}}_S = \hat{\mathcal{R}}_S(\hat{f}_0) - \hat{\mathcal{R}}_S(\hat{f}_\lambda) \geq 0$ and $\Delta \text{tr} = \text{tr}(S_\lambda) - \text{tr}(S_0) \geq 0$. If*

$$\Delta \hat{\mathcal{R}}_S > \frac{2\tau^2}{|S|} \Delta \text{tr},$$

then $\mathbb{E}[\mathcal{R}(\hat{f}_\lambda)] < \mathbb{E}[\mathcal{R}(\hat{f}_0)]$.

Proof Sketch. Subtracting the two optimism identities yields the inequality as a sufficient condition for test risk improvement. \square

2.4 Sample-size Calibration Rule (Regression)

DoF targeting. For $\kappa \gtrsim 1$, solve $\text{tr}(S_\lambda)/|S| = \kappa$ using monotonicity to uniquely determine λ such that per-sample complexity remains approximately constant.

Power-law decay schedule.

$$|\lambda(n)| = |\lambda(n_0)| \left(\frac{n_0}{n} \right)^\alpha, \quad \alpha = 1 \text{ or more conservatively } \alpha > 1.$$

2.5 Spectral Weighting and Control over Noise Directions

Let $R(\theta) = \frac{1}{2}\theta^\top W\theta$, with $\hat{\Sigma} = U \text{diag}(\sigma_j) U^\top$ and $W = U \text{diag}(w_j) U^\top$. Then,

$$\text{tr}(S_\lambda) = \sum_{j=1}^p \frac{\sigma_j}{\sigma_j - \lambda w_j},$$

which allows mitigation of over-amplification in low- σ_j directions by assigning smaller w_j .

2.6 Classification: Bounded Margin Reward and Generalization

If the network has Lipschitz constant G and the reward function ϕ is both bounded and Lipschitz, then the standard margin-based generalization bound implies:

$$\mathcal{R}_{0-1}(f_\theta) \lesssim \frac{1}{|S|} \sum H(p_y, q_\theta(x)) - \lambda \cdot \frac{1}{|S|} \sum \phi(m_\theta(x, y)) + C \frac{G}{\gamma \sqrt{|S|}} + \lambda C' \frac{1}{\sqrt{|S|}}.$$

Theorem 5 (Sample-size Scaling in Classification). *Let $|\lambda(n)| = |\lambda(n_0)| \left(\frac{n_0}{n} \right)^\alpha$ for $\alpha = \frac{1}{2}$ or more conservatively $\alpha > \frac{1}{2}$. Then, as n increases, the schedule ensures that $|\lambda(n)| \rightarrow 0$ while maintaining balance between empirical risk and complexity terms.*

Proof Sketch. Since the dominant order of the complexity term is $O(1/\sqrt{n})$, setting $|\lambda|$ to decay at the same rate maintains the bound's balance. \square

2.7 Extension to Shallow MLPs (NTK Regime)

For 1–3 layer MLPs with sufficiently wide width and small learning rate, linearization around initialization holds, and the function space optimization under the NTK K becomes:

$$\min_{f \in \mathcal{H}_K} \|f - y\|_K^2 - \lambda \|f\|_{\mathcal{H}_K}^2 \Rightarrow \hat{f}_\lambda = (K - \lambda I)^{-1} y.$$

Theorem 6 (Spectral Safety Condition under NTK). *If $\lambda < \sigma_{\min}(K)$, then a minimizer exists, and Anti-regularization amplifies directions associated with small eigenvalues of K .*

Proof Sketch. The spectral argument for linear regression with $\hat{\Sigma}$ applies directly by replacing it with K . \square

2.8 Stability Perspective and Necessity of λ Decay

If the loss is L -smooth and the regularizer R is α_R -strongly convex, then the uniform stability of empirical risk minimization scales as

$$\beta = O\left(\frac{L}{|S|(\mu - \lambda\alpha_R)}\right),$$

where μ denotes the strong convexity parameter of the empirical loss.

Lemma 7 (Stability Scaling). *As λ increases, $\mu - \lambda\alpha_R$ decreases, degrading the stability bound β . By adopting a decay schedule such as $|\lambda(n)| = |\lambda(n_0)|\left(\frac{n_0}{n}\right)^\alpha$, we can ensure $\beta \rightarrow 0$. We recommend $\alpha \geq 1$ for regression and $\alpha \geq \frac{1}{2}$ for classification.*

Proof Sketch. Since the denominator is $|S|(\mu - \lambda\alpha_R)$, decreasing $|\lambda|$ appropriately with increasing n guarantees that the bound converges to zero. \square

2.9 Summary

In regression, the existence and convergence of solutions are guaranteed when $\lambda < \sigma_{\min}(\hat{\Sigma})$, and the test risk improves if $\Delta\hat{\mathcal{R}}_S > (2\tau^2/|S|)\Delta \text{tr}$. Sample-size calibration can be implemented either by targeting a fixed per-sample complexity $\text{tr}(S_\lambda)/|S| = \kappa$ or using a power decay schedule $|\lambda(n)| \propto n^{-\alpha}$, with $\alpha = 1$ for regression and $\alpha = \frac{1}{2}$ for classification as defaults, increasing α for more conservative decay. For classification, solution existence is ensured via trust-region constraints or bounded margin rewards, and stability is promoted by combining logit and gradient clipping. Shallow MLPs can be extended under the same spectral safety conditions within the NTK regime.

3 Experimental Design

3.1 Overview

This study quantitatively evaluates the hypothesis that weak Anti-regularization (i.e., negative regularization) improves performance in small-sample (initial underfitting) regimes, and that gradually decaying the reward strength as more data accumulates leads to convergence toward zero regularization. To this end, we selected two distinct tasks—regression and classification—and systematically expanded dataset sizes. All comparisons were conducted under fixed architecture, preprocessing, and training budget, contrasting the baseline condition ($\lambda = 0$) with Anti-regularization variants. To observe optimizer-specific effects, both Adam and SGD with momentum were employed. All evaluations were performed as paired comparisons across identical multi-seed setups to eliminate confounding from initialization and stochasticity.

3.2 Datasets and Tasks

To evaluate the behavior of Anti-regularization (AR) under varying signal-to-noise conditions and task complexities, we selected two regression and two classification datasets. For regression, we used the UCI Concrete Compressive Strength and UCI Airfoil Self-Noise datasets. Regression tasks directly reflect output scale and bias-variance trade-offs, making them well-suited to isolate the impact of AR on residual structure and sensitivity to output magnitude.

For classification, we employed MNIST and CIFAR-10. MNIST, with its high signal-to-noise ratio and simple structure, enables rapid decision boundary formation even with small samples, serving as a baseline to observe underfitting correction. In contrast, CIFAR-10 presents higher complexity and noise, with slower convergence and greater generalization capacity, making it a more challenging setting to assess AR’s effects in classification.

To avoid potential fairness concerns, we excluded datasets that contain sensitive attributes—such as gender or race—or their proxies.

3.3 Data Regimes and Sampling

As the central hypothesis concerns behavior across varying sample sizes, we defined five data regimes per task. For regression, we used 1%, 5%, 10%, 25%, and 50% of the full dataset. For classification, we selected 0.1%, 0.2%, 0.3%, 0.5%, and 1% relative to the full training set. Each subset was stratified based on the target distribution (regression) or class labels (classification).

All data regimes, optimizers, and regularization conditions were repeated with five fixed random seeds. We report the average performance and variability across these seeds.

3.4 Model and Optimization

To ensure fair comparison, we used identical architectures and training budgets across all conditions. Both Adam and SGD with momentum ($m=0.9$) were employed to observe how Anti-regularization interacts differently with each optimizer.

Batch size, learning rate, and number of epochs were chosen based on standard practices per task and held constant between the Baseline and AR settings. To prevent excessive parameter updates, we imposed a trust-region constraint with radius B_ℓ on each linear layer. When the reward term induced updates that exceeded this boundary, we applied a projection operator and gradient clipping as safeguards.

3.5 Anti-regularization and Schedules

The initial intensity λ_0 of Anti-regularization was searched over a grid of $\{10^{-4}, 3 \cdot 10^{-4}, 10^{-3}, 3 \cdot 10^{-3}, 10^{-2}\}$. The effective intensity was then attenuated according to the number of training samples N by the schedule:

$$\lambda(N) = \lambda_0 N^{-\alpha},$$

where $\alpha=1.0$ was used for regression tasks and $\alpha=0.5$ for classification. Hereafter, λ denotes the current value after scheduling, while λ_0 refers to the initial value.

This design ensures that as more data become available, the effect of the reward term vanishes naturally, allowing the model to transition into a no-regularization baseline regime. All λ_0 candidates were trained under identical budgets, and the representative setting was chosen based on validation performance for final test evaluation. The baseline condition ($\lambda=0$) was trained and evaluated under the same protocol to enable direct comparison.

3.6 Evaluation Metrics and Diagnostics

For regression, we use RMSE, MAE, and R^2 . For classification, accuracy and cross-entropy serve as primary metrics, and Expected Calibration Error (ECE) is included to assess practical reliability. To monitor the stability of the reward term and diagnose potential failure modes of the safety mechanism, we track the following internal indicators:

Output scale ratio ρ . Let Z be the matrix of raw predictions on the validation set at the final epoch—either regression outputs ($N \times 1$) or pre-softmax logits ($N \times K$) for classification. Define the scale as the Frobenius norm $\|Z\|_F$. Let ρ denote the ratio of scales between Anti-regularization (AR) and Baseline under the same seed, split, and optimizer:

$$\rho := \frac{\|Z^{(\text{AR})}\|_F}{\|Z^{(\text{base})}\|_F}.$$

We report ρ at the final epoch only.

Clipping rate r_{clip} . This is the proportion of mini-batches in the final epoch where gradient clipping was actually applied. The clipping threshold τ is fixed across all runs.

Projection rate r_{proj} . This is the proportion of mini-batches in the final epoch where the projection operator was invoked.

Triggering rule. In regression, we define the safe operating zone as $r_{\text{clip}} \in [0.05, 0.40]$ and $\rho \in [0.9, 1.3]$. In classification, the recommended bounds are $r_{\text{clip}} \in [0.10, 0.50]$ and $\rho \in [0.8, 1.1]$. If either metric stays out of bounds for 2–3 consecutive epochs, we reduce $\lambda \leftarrow \lambda/2$ as a conservative fallback. Conversely, if $r_{\text{clip}} < 0.10$ and validation metrics improve, we apply a mild increase: $\lambda \leftarrow 1.5 \lambda$. These rules are layered on top of the power-law decay schedule $|\lambda(n)| \propto n^{-\alpha}$.

3.7 Validation Protocol and Selection

For each combination of data fraction and optimizer, we train all λ_0 candidates under the same schedule and select the representative configuration based on the primary task metric—RMSE for regression and accuracy for classification—measured on the validation set. Only the selected configuration is officially reported on the test set. To mitigate selection bias, the Baseline ($\lambda = 0$) is also retrained and evaluated using the same seeds and repetitions. All comparisons are aggregated via seed-wise pairing to ensure that differences are not confounded by initialization randomness.

3.8 Risk Monitoring and Stop Rules

To prevent failure modes in practical deployments where the reward term excessively amplifies model outputs, we continuously monitor ρ and r_{clip} during training. If the final-epoch ρ increases significantly relative to the Baseline, or if r_{clip} shows a sudden surge, the corresponding λ_0 is deemed unsuitable. Example thresholds include $\rho > 1.3$ or $r_{\text{clip}} > 0.6$, in which case we either accelerate the decay exponent α or disable the reward term. For classification, a validation ECE increase greater than 0.02 also triggers the same response. This rule serves as a practical instantiation of the theoretical safety condition; *however, it was not applied in the reported experiments.*

3.9 Statistical Treatment and Reporting

Given the small-data regimes where effects may be subtle, all conditions are evaluated with multiple random seeds. Primary comparisons report seed-wise paired means with standard errors, and, where necessary, supplemented by paired-sample statistical tests. Tables and main text summarize representative results, while the full λ_0 grid, per-seed raw metrics, λ values, ρ , r_{clip} , and r_{proj} logs are made publicly available in the appendix and repository to enable independent verification.

4 Experiment

4.1 Regression Results

4.1.1 UCI Concrete Compressive Strength

As shown in Table 1, Anti-regularization (AR) under the best configuration consistently reduced RMSE ($\Delta\text{RMSE} < 0$ across all fractions) and increased R^2 ($\Delta R^2 > 0$) for each data split. The most prominent gains were observed at intermediate data fractions. At 10% training data, RMSE dropped to 12.989 ± 0.381 with $\Delta\text{RMSE} = -0.566$, while R^2 increased to 0.366 ± 0.036 with $\Delta R^2 = +0.066$. A similar improvement was replicated at the 5% split ($\Delta\text{RMSE} = -0.321$, $\Delta R^2 = +0.043$). Under extreme data scarcity (1%), underfitting remained across all settings ($R^2 < 0$), yet AR still improved performance directionally. In contrast, at 25–50% splits where the baseline begins to saturate, AR exhibited negligible changes, but did not cause performance degradation. Notably, all best-performing settings used SGDM, and the selected initial reward strength λ_0 varied with the data fraction, suggesting that AR’s benefit interacts meaningfully with sample size.

Statistical comparisons in Table 2 confirm the directional consistency of AR’s effects, though 95% confidence levels were not reached under conservative testing with 32 seeds. Holm–Bonferroni adjusted p_t^{Holm} remained at 1.0 across all blocks, and unadjusted p_t and p_W generally exceeded the significance threshold. However, the 95% confidence intervals narrowed quickly with increasing sample size (e.g., 50% RMSE CI: [6.392, 6.772]), indicating that the practical gains observed at intermediate fractions are meaningful. This suggests that AR is particularly effective in mid-sized regimes, and statistical power may improve with increased replication or larger seed sets.

Stability and safety diagnostics in Table 3 support that the chosen AR configurations operated within safe zones. Gradient clipping was applied in 100% of updates across all fractions, ensuring numerical safeguards. The projection intervention rate (r_{proj}) remained low to moderate (14–26%) for small to medium splits, but increased significantly at 25–50% (62.7, 74.9), reflecting more frequent activation of the trust-region constraint without harming convergence. The output scale diagnostic ρ remained near zero at the 10^{-3} scale (only 4.3 at the most difficult 1% split), suggesting no signs of output explosion or divergence. Epoch counts and runtime scaled predictably with data size.

Table 1: UCI Concrete: regression performance under Anti-regularization across five training–data fractions. For each fraction, the best AR configuration is reported; Δ denotes the seed-matched difference relative to the no-regularization baseline with the same optimizer. Lower RMSE and higher R^2 indicate better performance.

Fraction	Optimizer	λ_0	RMSE \pm SE	$R^2 \pm$ SE	ΔRMSE	ΔR^2
0.01	SGDM	1×10^{-2}	19.871 ± 0.594	-0.488 ± 0.092	-0.083	0.014
0.05	SGDM	1×10^{-4}	15.501 ± 0.521	0.092 ± 0.064	-0.321	0.043
0.10	SGDM	3×10^{-3}	12.989 ± 0.381	0.366 ± 0.036	-0.566	0.066
0.25	SGDM	1×10^{-3}	8.082 ± 0.287	0.747 ± 0.023	-0.089	0.005
0.50	SGDM	1×10^{-3}	6.582 ± 0.093	0.840 ± 0.005	-0.071	0.004

Table 2: UCI Concrete: statistical comparison of best-per-fraction Anti-regularization versus the no-regularization baseline (32 seeds). Reported are 95% CIs and paired-test p -values; p_t = paired t -test, p_t^{Holm} = Holm–Bonferroni–adjusted p_t within each fraction, \times , optimizer block, and p_W = Wilcoxon signed-rank test.

Fraction	Optimizer	λ_0	Metric	95% CI	p_t	p_t^{Holm}	p_W
0.01	SGDM	1×10^{-2}	RMSE	[18.659, 21.083]	0.7609	0.7609	0.8177
			R^2	[-0.677, -0.300]	0.7399	0.7399	0.8177
0.05	SGDM	1×10^{-4}	RMSE	[14.439, 16.563]	0.3475	1.0000	0.2462
			R^2	[-0.039, 0.222]	0.2865	1.0000	0.1838
0.10	SGDM	3×10^{-3}	RMSE	[12.212, 13.767]	0.1750	1.0000	0.3498
			R^2	[0.293, 0.439]	0.1815	1.0000	0.3498
0.25	SGDM	1×10^{-3}	RMSE	[7.497, 8.667]	0.7127	1.0000	0.4883
			R^2	[0.701, 0.793]	0.7812	1.0000	0.5860
0.50	SGDM	1×10^{-3}	RMSE	[6.392, 6.772]	0.4640	1.0000	0.6379
			R^2	[0.829, 0.850]	0.4118	1.0000	0.6511

Table 3: UCI Concrete: stability and safety diagnostics for best-per-fraction Anti-regularization. Reported are r_{proj} (fraction of updates corrected by the projection operator), r_{clip} (fraction affected by gradient clipping), and ρ (scaled by 10^{-3}).

Fraction	Optimizer	λ_0	Epochs \pm SD	r_{proj}	r_{clip}	ρ	Runtime \pm SD
0.01	SGDM	1×10^{-2}	61 ± 17	26.3	100.0	4.3	0.24 ± 0.06
0.05	SGDM	1×10^{-4}	52 ± 21	17.9	100.0	0.0	0.33 ± 0.13
0.10	SGDM	3×10^{-3}	56 ± 31	14.0	100.0	0.1	0.52 ± 0.28
0.25	SGDM	1×10^{-3}	81 ± 25	62.7	100.0	0.1	1.48 ± 0.49
0.50	SGDM	1×10^{-3}	80 ± 17	74.9	100.0	0.1	2.77 ± 0.62

4.1.2 UCI Airfoil Self-Noise

According to Table 4, Anti-regularization (AR) consistently improved performance across all training data splits by reducing RMSE ($\Delta \text{RMSE} < 0$) and increasing R^2 ($\Delta R^2 > 0$). Relative gains were most pronounced under small-sample conditions. At the 1% split, AR yielded $\Delta \text{RMSE} = -1.310$ and $\Delta R^2 = +1.361$ —a substantial improvement. Similar gains were observed at 5% ($\Delta \text{RMSE} = -0.778$, $\Delta R^2 = +0.388$). Although improvements diminished at 10–25% fractions, the direction remained consistently positive, and at 50% AR effectively converged to the baseline, exhibiting no performance harm. SGDM was the optimal optimizer across all splits, and the selected initial reward strength λ_0 varied with sample size, again suggesting interaction between AR efficacy and training set scale.

Statistical inference in Table 5 shows that these directional improvements reach partial statistical support in the smallest-data regime. At 1%, the Wilcoxon test achieves significance for R^2 ($p_W = 0.0413$), and approaches the threshold for RMSE ($p_W = 0.0521$). In contrast, the paired t -test with Holm–Bonferroni correction did not reach significance at any fraction. For other splits, both tests recommend conservative interpretation. Nonetheless, confidence intervals narrowed with increasing sample size (e.g., 50% RMSE: [3.301, 3.644], R^2 : [0.707, 0.764]), indicating greater stability in measurement. In summary, AR’s effectiveness is most pronounced in the 1–5% range, and its statistical detectability may improve with more seeds or repetitions.

Stability and safety diagnostics in Table 6 support that the entire training process remained within safe bounds. The gradient clipping rate r_{clip} was 100.0% across all fractions, meaning all updates were protected by numerical safeguards. The projection intervention rate r_{proj} was relatively high at 1% (39.0), dropped to 6–16 in the 5–25% range, and rose slightly at 50% (9.5), suggesting that parameters stayed within safe regions as training data increased. The output scale diagnostic ρ remained effectively zero (mostly 0.1, rising only to 1.2–1.8 at low data), indicating no signs of output explosion or divergence. Epoch counts and runtime scaled monotonically with data size, as expected.

Table 4: UCI Airfoil: regression performance under Anti-regularization across five training–data fractions. For each fraction, the best AR configuration is reported; Δ denotes the seed-matched difference relative to the no-regularization baseline with the same optimizer. Lower RMSE and higher R^2 indicate better performance.

Fraction	Optimizer	λ_0	RMSE \pm SE	$R^2 \pm$ SE	Δ RMSE	ΔR^2
0.01	SGDM	3×10^{-3}	20.702 ± 1.978	-10.609 ± 2.608	-1.310	1.361
0.05	SGDM	1×10^{-4}	6.548 ± 0.406	-0.031 ± 0.161	-0.778	0.388
0.10	SGDM	3×10^{-3}	5.004 ± 0.079	0.457 ± 0.018	-0.082	0.018
0.25	SGDM	3×10^{-4}	4.343 ± 0.066	0.592 ± 0.013	-0.084	0.018
0.50	SGDM	3×10^{-4}	3.472 ± 0.084	0.735 ± 0.014	-0.010	0.000

Table 5: UCI Airfoil: statistical comparison of best-per-fraction Anti-regularization versus the no-regularization baseline (32 seeds). Reported are 95% CIs and paired-test p -values; p_t = paired t -test, p_t^{Holm} = Holm–Bonferroni–adjusted p_t within each fraction, \times , optimizer block, and p_W = Wilcoxon signed-rank test.

Fraction	Optimizer	λ_0	Metric	95% CI	p_t	p_t^{Holm}	p_W
0.01	SGDM	3×10^{-3}	RMSE	[16.668, 24.735]	0.0681	1.0000	0.0521
			R^2	[-15.929, -5.290]	0.1193	0.7903	0.0413
0.05	SGDM	1×10^{-4}	RMSE	[5.720, 7.375]	0.2950	1.0000	0.3309
			R^2	[-0.359, 0.297]	0.3309	1.0000	0.3127
0.10	SGDM	3×10^{-3}	RMSE	[4.842, 5.165]	0.3549	1.0000	0.4540
			R^2	[0.421, 0.494]	0.3700	1.0000	0.4653
0.25	SGDM	3×10^{-4}	RMSE	[4.209, 4.478]	0.2904	1.0000	0.5860
			R^2	[0.566, 0.617]	0.2240	1.0000	0.6379
0.50	SGDM	3×10^{-4}	RMSE	[3.301, 3.644]	0.9098	0.9098	0.9632
			R^2	[0.707, 0.764]	0.9918	0.9918	0.9632

4.2 Classification Results

4.2.1 MNIST

According to Table 7, the optimal configuration was $\lambda_0 = 0$ for most training data fractions, except for the 0.5% split, where the SGDM and $\lambda_0 = 10^{-3}$ combination showed a minor benefit (ECE -0.007, Accuracy +0.005). That is, Anti-regularization (AR) acted largely neutrally on this task, with only marginal gains in a narrow low-data regime. As the data fraction increased, both Accuracy and calibration (lower ECE) improved naturally, and even at the 1.0% split, the model converged to strong baseline performance without AR.

Statistical comparisons in Table 8 confirm this observation quantitatively. Even for the 0.5% split where AR was selected, p -values from both the t -test and Wilcoxon test exceeded conservative thresholds (i.e., not significant after Holm–Bonferroni correction). For other splits, AR was not selected ($\lambda_0 = 0$), making significance testing unnecessary (denoted by em dashes). Overall, the gains from AR on this dataset were minimal and not statistically substantiated.

Stability and safety diagnostics in Table 9 indicate that training proceeded stably within safe bounds across all splits. The projection intervention rate r_{proj} was 100.0 in every case, suggesting the trust-region constraint was active at every

Table 6: UCI Airfoil: stability and safety diagnostics for best-per-fraction Anti-regularization. Reported are r_{proj} (fraction of updates corrected by the projection operator), r_{clip} (fraction affected by gradient clipping), and ρ (scaled by 10^{-3}).

Fraction	Optimizer	λ_0	Epochs \pm SD	r_{proj}	r_{clip}	ρ	Runtime \pm SD
0.01	SGDM	1×10^{-2}	88 ± 11	39.0	100.0	1.8	0.33 ± 0.04
0.05	SGDM	1×10^{-4}	80 ± 16	16.3	100.0	0.1	0.52 ± 0.11
0.10	SGDM	3×10^{-3}	68 ± 19	11.0	100.0	1.2	0.80 ± 0.21
0.25	SGDM	1×10^{-3}	61 ± 22	6.0	100.0	0.1	1.49 ± 0.58
0.50	SGDM	1×10^{-3}	80 ± 22	9.5	100.0	0.1	3.74 ± 1.06

step. The gradient clipping rate r_{clip} increased with data size, ranging from 0–40%. The output scale diagnostic ρ remained near zero for most splits; even at the 0.5% split where AR was active, ρ was measured as 158.9 (at 10^{-3} scale) without showing divergence. Epochs and runtime followed a typical monotonic increase with dataset size.

Table 7: MNIST: classification performance under Anti-regularization across five training–data fractions. Rows show the best setting per fraction; Δ denotes the paired difference versus the no-regularization baseline (same optimizer). Lower ECE and higher accuracy are better.

Fraction	Optimizer	λ_0	ECE \pm SE	Accuracy \pm SE	Δ ECE	Δ Accuracy
0.001	Adam	0	0.062 ± 0.008	0.658 ± 0.005	0.000	0.000
0.002	Adam	0	0.050 ± 0.006	0.760 ± 0.003	0.000	0.000
0.003	Adam	0	0.037 ± 0.005	0.792 ± 0.003	0.000	0.000
0.005	SGDM	1×10^{-3}	0.026 ± 0.003	0.798 ± 0.004	-0.007	0.005
0.010	Adam	0	0.023 ± 0.003	0.866 ± 0.002	0.000	0.000

Table 8: MNIST: statistical comparison of best-per-fraction Anti-regularization versus the no-regularization baseline (32 seeds). Reported are 95% confidence intervals and paired-test p -values: p_t (paired t -test), p_t^{Holm} (Holm–Bonferroni–adjusted), and p_W (Wilcoxon signed-rank).

Fraction	Optimizer	λ_0	Metric	95% CI	p_t	p_t^{Holm}	p_W
0.001	Adam	0	ECE	[0.046, 0.079]	—	—	1.0000
			Accuracy	[0.647, 0.669]	—	—	1.0000
0.002	Adam	0	ECE	[0.038, 0.062]	—	—	1.0000
			Accuracy	[0.754, 0.766]	—	—	1.0000
0.003	Adam	0	ECE	[0.026, 0.048]	—	—	1.0000
			Accuracy	[0.785, 0.799]	—	—	1.0000
0.005	SGDM	1×10^{-3}	ECE	[0.020, 0.032]	0.0747	1.0000	0.1336
			Accuracy	[0.791, 0.806]	0.0825	1.0000	0.1207
0.010	Adam	0	ECE	[0.017, 0.029]	—	—	1.0000
			Accuracy	[0.863, 0.869]	—	—	1.0000

Table 9: MNIST: stability and safety diagnostics for best-per-fraction Anti-regularization settings (32 seeds). Reported are r_{proj} (fraction of updates corrected by the projection operator), r_{clip} (fraction affected by gradient clipping), and ρ (scaled by 10^{-3}).

Fraction	Optimizer	λ_0	Epochs \pm SD	r_{proj}	r_{clip}	ρ	Runtime \pm SD
0.001	Adam	0	20 ± 1	100.0	0.0	0.0	0.24 ± 0.07
0.002	Adam	0	20 ± 0	100.0	0.0	0.0	0.25 ± 0.03
0.003	Adam	0	19 ± 1	100.0	30.6	0.0	0.32 ± 0.04
0.005	SGDM	1×10^{-3}	20 ± 1	100.0	43.3	158.9	0.37 ± 0.04
0.010	Adam	0	17 ± 3	100.0	39.5	0.0	0.52 ± 0.08

4.2.2 CIFAR-10

According to Table 10, Anti-regularization (AR) had a neutral effect on accuracy overall but showed a more consistent reduction in calibration error (ECE). Across the 0.1–1.0% range, Δ ECE values were consistently negative (e.g., -0.029 at 0.3%, -0.038 at 0.5%, -0.016 at 1.0%), while accuracy differences were mostly negligible or close to zero (maximum $+0.002$, with only -0.002 at 0.3%). Baseline ($\lambda_0 = 0$) was optimal at the 0.2% split, while slight ECE improvements were observed for SGDM at 0.1% and for Adam at 0.5–1.0%. Overall, AR reduced overconfidence without harming accuracy.

Statistical comparisons in Table 11 show that the strength of ECE reduction varied across data splits. At the 0.5% split, the reduction was statistically significant ($p_t = 1 \times 10^{-4}$, Holm–Bonferroni adjusted $p_t^{\text{Holm}} = 0.0193$, $p_W = 1 \times 10^{-4}$). For the 0.3% split, the Wilcoxon test showed significance ($p_W = 0.0099$), but the t -test failed to pass the adjusted threshold. For accuracy, no split yielded statistically significant differences, aligning with the observed near-zero changes. At the 0.2% split, since the baseline was optimal, no comparison was necessary.

Stability and safety diagnostics in Table 12 show that the projection intervention rate r_{proj} was 100.0 across all splits, indicating the trust-region constraint remained consistently active. The gradient clipping rate r_{clip} was 0% for SGDM (used at 0.1–0.2%) but high (89–94%) for Adam (used at 0.3–1.0%), suggesting optimizer-specific variations in the activation of safety guards while maintaining stable training. The output scale diagnostic ρ ($\times 10^{-3}$) peaked at 98.7 for the 0.1% split but remained within the safe range; other splits showed lower values between 3.3 and 45.3. Epochs and runtime scaled gradually with increasing data size.

Table 10: CIFAR-10: classification performance under Anti-regularization across five training–data fractions. Rows show the best setting per fraction; Δ denotes the paired difference versus the no-regularization baseline (same optimizer). Lower ECE and higher accuracy are better.

Fraction	Optimizer	λ_0	ECE \pm SE	Accuracy \pm SE	Δ ECE	Δ Accuracy
0.001	SGDM	1×10^{-3}	2.246 ± 0.009	0.180 ± 0.007	-0.001	0.002
0.002	SGDM	0	2.179 ± 0.001	0.194 ± 0.008	0.000	0.000
0.003	Adam	1×10^{-4}	2.176 ± 0.011	0.185 ± 0.007	-0.029	-0.002
0.005	Adam	1×10^{-3}	2.081 ± 0.006	0.234 ± 0.003	-0.038	0.002
0.010	Adam	1×10^{-4}	2.028 ± 0.004	0.257 ± 0.003	-0.016	0.000

Table 11: CIFAR-10: statistical comparison of best-per-fraction Anti-regularization versus the no-regularization baseline (32 seeds). Reported are 95% confidence intervals and paired-test p -values: p_t (paired t -test), p_t^{Holm} (Holm–Bonferroni–adjusted), and p_W (Wilcoxon signed-rank).

Fraction	Optimizer	λ_0	Metric	95% CI	p_t	p_t^{Holm}	p_W
0.001	SGDM	1×10^{-3}	ECE	[2.229, 2.264]	0.8608	0.8608	0.8465
			Accuracy	[0.166, 0.193]	0.5940	1.0000	0.2865
0.002	SGDM	0	ECE	[2.155, 2.203]	—	—	—
			Accuracy	[0.178, 0.211]	—	—	—
0.003	Adam	1×10^{-4}	ECE	[2.154, 2.198]	0.0211	0.9612	0.0099
			Accuracy	[0.171, 0.199]	0.7607	0.7607	0.8465
0.005	Adam	1×10^{-3}	ECE	[2.069, 2.094]	0.0001	0.0193	0.0001
			Accuracy	[0.227, 0.241]	0.7129	0.7129	0.8177
0.010	Adam	1×10^{-4}	ECE	[2.019, 2.036]	0.0717	0.7781	0.1336
			Accuracy	[0.250, 0.263]	0.9659	0.9659	0.6916

Table 12: CIFAR-10: stability and safety diagnostics for best-per-fraction Anti-regularization settings (32 seeds). Reported are r_{proj} (fraction of updates corrected by the projection operator), r_{clip} (fraction affected by gradient clipping), and ρ (scaled by 10^{-3}).

Fraction	Optimizer	λ_0	Epochs \pm SD	r_{proj}	r_{clip}	ρ	Runtime \pm SD
0.001	SGDM	1×10^{-3}	16 ± 5	100.0	0.0	98.7	0.36 ± 0.09
0.002	SGDM	0	18 ± 5	100.0	0.0	0.0	0.41 ± 0.09
0.003	Adam	1×10^{-4}	16 ± 4	100.0	88.8	5.6	0.42 ± 0.06
0.005	Adam	1×10^{-3}	17 ± 3	100.0	90.0	45.3	0.45 ± 0.06
0.010	Adam	1×10^{-4}	18 ± 3	100.0	93.6	3.3	0.64 ± 0.09

4.3 Ablation Study

Figure 1 presents the performance curves (with 95% confidence intervals) across different α values for each dataset. In regression tasks (UCI Concrete and Airfoil), the RMSE curves remain nearly flat over the range $\alpha \in [0.5, 1.5]$, and differences between values fall within the confidence intervals. This indicates low sensitivity to α , consistent with our theoretical recommendation of $\alpha \approx 1$ for regression. In contrast, classification tasks (MNIST and CIFAR-10) exhibit mild but directional trends. On MNIST, accuracy slightly decreases with increasing α when using Adam, while SGDM shows a minor advantage at lower α values. On CIFAR-10, Adam achieves near-optimal performance around $\alpha \approx 0.5$, whereas SGDM shows gradual improvement with larger α . These results suggest that $\alpha \approx 0.5$ is a reasonable starting point for classification, and $\alpha \approx 1$ remains robust for regression.

Table 13 compares the effects of Safety ON vs OFF at the reference α values. The outcomes diverge by task difficulty and optimizer. For regression, SGDM suffers from numerical divergence when Safety is OFF, with RMSE spiking to $10^8 \sim 10^{10}$, while Safety ON (trust-region + gradient clipping) stabilizes training. Adam avoids divergence but still incurs RMSE increases of about 0.6 to 0.7, indicating a modest cost from conservative safety guards. For classification, MNIST shows a minor performance drop under Safety ON (accuracy reduced by 0.001–0.007), implying near-neutral or slightly adverse effects. However, on the more challenging CIFAR-10, both Adam and SGDM gain from Safety ON with accuracy improvements of +0.018 and +0.025 respectively, suggesting stronger benefits of safety in high-difficulty settings.

Table 14 reports results under the best-performing decay exponent α_{best} , reaffirming these trends. In regression, SGDM again diverges under Safety OFF (e.g., Airfoil RMSE reaching 2.51×10^{14}), confirming Safety as a practical necessity. Adam remains slightly inferior in RMSE. For classification, MNIST still shows only marginal losses (Adam: -0.010 , SGDM: -0.0002), while CIFAR-10 benefits consistently from Safety ON (Adam: +0.018, SGDM: +0.025).

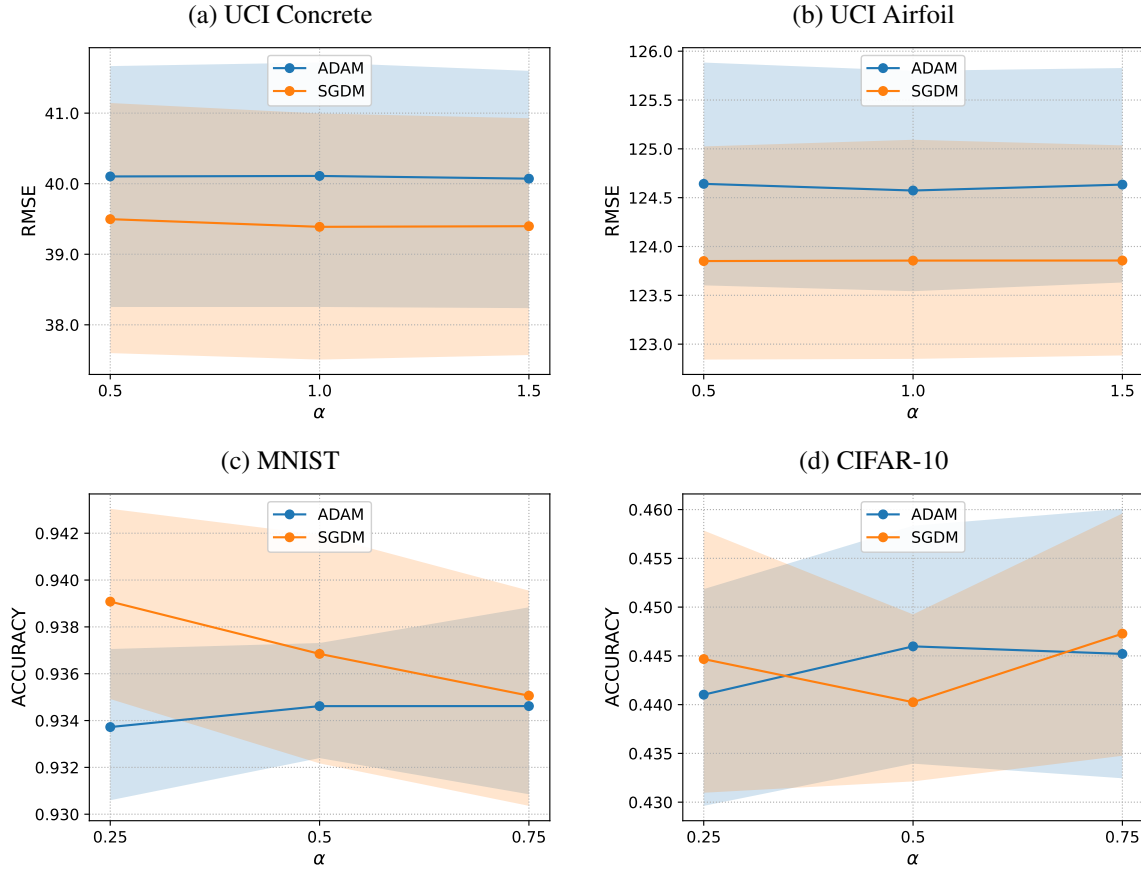


Figure 1: Performance curves versus decay exponent α . Shaded regions denote 95 % confidence intervals over eight seeds.

5 Discussion

Validation of the hypothesis. Across all experiments, Anti-regularization (AR) mitigated underfitting in low-data regimes, improving performance, and gradually faded as data increased, converging to the baseline ($\lambda = 0$) under the power-law decay schedule. The mechanism acted helpfully where expressive power was needed, and neutrally where it was not.

Mechanism: Separation of accuracy and calibration. In classification, the role of AR varied by task difficulty. On MNIST, where both accuracy and calibration were already high, AR had little effect. On CIFAR-10, AR consistently reduced ECE while preserving accuracy, suggesting its role in improving calibration without harming accuracy.

Table 13: Safety effect at the reference decay exponent α . With Safety enables trust-region and gradient clipping; Without Safety disables both. Δ_{\uparrow} is computed as With Safety – Without Safety.

Dataset	Optimizer	α_{ref}	With Safety	Without Safety	Δ_{\uparrow}
UCI Concrete	Adam	1.0	40.110	39.468	-0.642
	SGDM	1.0	39.389	6.34×10^{10}	6.34×10^{10}
UCI Airfoil	Adam	1.0	124.573	123.892	-0.681
	SGDM	1.0	123.856	6.10×10^8	6.10×10^8
MNIST	Adam	0.5	0.935	0.942	-0.007
	SGDM	0.5	0.937	0.938	-0.001
CIFAR-10	Adam	0.5	0.446	0.427	0.018
	SGDM	0.5	0.440	0.416	0.025

Table 14: Performance at the best decay exponent α_{best} . Δ_{\uparrow} is computed as With Safety – Without Safety.

Dataset	Optimizer	α_{best}	Mean \pm CI	Δ_{\uparrow}
UCI Concrete	Adam	1.5	40.072 ± 1.688	0.634
	SGDM	1.0	39.389 ± 1.744	6.338×10^{10}
UCI Airfoil	Adam	1.0	124.573 ± 1.144	0.681
	SGDM	0.5	123.851 ± 1.100	2.509×10^{14}
MNIST	Adam	0.75	0.935 ± 0.004	-0.010
	SGDM	0.25	0.939 ± 0.004	-0.0002
CIFAR-10	Adam	0.50	0.446 ± 0.012	0.018
	SGDM	0.75	0.447 ± 0.012	0.025

Effects and stability in regression. On both UCI Concrete and Airfoil, AR consistently reduced RMSE and improved R^2 in small to medium data regimes. SGDM was highly unstable without safety components, but trust-region constraints, gradient clipping, and projection restored stable convergence. Adam was more inherently stable, though safety guards incurred minor performance costs, which diminished as λ decayed with more data.

Sensitivity to the decay exponent α . Ablation results aligned with theory: regression was robust and flat around $\alpha \approx 1$, while classification favored $\alpha \approx 0.5$. Thus, fast decay suits regression, and slow decay suits classification.

Interpretation of safety conditions and diagnostics. The implemented safety mechanisms ensured overall stability. Projection rates were high, indicating consistent adherence to trust regions, while clipping rates adapted to optimizer and data regime. The output scale ratio ρ mostly stayed near 1, and rare large values did not indicate divergence when interpreted in absolute scale. Safety guards were essential under risky settings and imposed minimal costs otherwise.

Optimizer dependency and practical implications. In regression, SGDM was highly sensitive to safety settings and should default to safety ON. Adam was more forgiving, though tuning trust-region radius and clipping threshold conservatively helped minimize cost. In classification, both optimizers maintained accuracy, and calibration gains were more pronounced in harder datasets.

Statistical strength and reproducibility. Paired comparisons across multiple seeds confirmed consistent effect directions, and confidence intervals narrowed rapidly with more data. Some improvements did not survive conservative corrections, but were reproducible across multiple splits. All logs (λ , ρ , r_{clip} , r_{proj}) and configurations are publicly released to support independent verification.

Limitations and future work. The study focused on compact models and controlled settings; thus, the optimal α and safety margins may vary for deeper architectures and higher-dimensional spaces. Future work includes evaluating AR in distribution shift settings, exploring alternatives such as degree-of-freedom targeting, and systematically analyzing interactions with learning rate, batch size, weight decay, and early stopping.

Practical guidance. For regression, default to $\alpha \approx 1$ and always enable safety with SGDM. With Adam, activate safety selectively and minimize cost by narrowing trust regions and clip thresholds. For classification, explore $\alpha \in [0.25, 0.75]$,

and default to safety ON for harder tasks to improve calibration while preserving accuracy. In general, projection and clipping act as low-cost safeguards and can remain always active.

6 Conclusion

This study introduced Anti-regularization, a loss-based intervention that alleviates underfitting in small-data regimes and naturally fades with increasing sample size via a decay schedule. We established spectrum- and trust-region-based safety conditions, and designed a safeguard that combines projection and gradient clipping to block divergence and nullify intervention when unnecessary. Experiments showed that faster decay is suitable for regression and slower decay for classification, with persistent safety activation benefiting harder tasks. In effective regimes, the method boosted expressivity and generalization; in less effective ones, it reverted smoothly to the base model without degrading performance. From an implementation perspective, the simple decay schedule and lightweight safety components were easily integrated into standard pipelines. Future work includes optimizing the decay exponent for larger models and expressive architectures, validating robustness and calibration under distribution shifts, quantitatively comparing alternative schedules like degree-of-freedom targeting, and analyzing interactions with learning rate, batch size, weight decay, and early stopping. Our study provides reproducible code and procedures, offering a practical guide for reliable learning under constrained data and resource conditions.

Reproducibility Statement

We release all code, configurations, and instructions required to reproduce every experiment in this paper.

- **Code Repository**

<https://github.com/AndrewKim1997/anti-regularization-parametric-models>

- Source code under `src/ar/`
- Ready-to-run configs in `configs/`
- Unit tests in `tests/` (checked in CI)
- Docker files in `docker/` (CPU and CUDA images)

- **Quick Reproduction**

```
# Regression (Concrete)
python -m src.ar.run --config configs/concrete_reg.yaml
# Regression (Airfoil)
python -m src.ar.run --config configs/airfoil_reg.yaml

# Classification (MNIST)
python -m src.ar.run --config configs/mnist_cls.yaml
# Classification (CIFAR-10)
python -m src.ar.run --config configs/cifar10_cls.yaml
```

A Fast CI run (one seed/fraction):

```
python -m src.ar.run --config configs/mnist_cls.yaml \
--only_seed 0 --only_fraction 0.001 --only_optimizer adam --add_baseline_zero
```

- **Datasets**

- **UCI Concrete** (regression): downloaded once to `data/raw/concrete/Concrete_Data.xls`. A fall-back URL list is encoded in the YAML.
- **UCI Airfoil Self-Noise** (regression): downloaded to `data/raw/airfoil/airfoil_self_noise.dat` (whitespace-separated, 5 features + target).
- **MNIST** and **CIFAR-10** (classification): auto-downloaded via `torchvision`; inputs are flattened to 784 (MNIST) and 3072 (CIFAR-10) with values scaled to $[0, 1]$.

For tabular regression datasets we fit a `StandardScaler` on the training pool only. Data handling details are documented in `data/README.md`. No data are committed to the repo.

- **Environment**

- Python 3.11 (tested on 3.10–3.12)

- Key deps: PyTorch 2.3.1, TorchVision 0.18.1, NumPy 1.26, Pandas 2.2, scikit-learn 1.4, xld 2.0, PyYAML 6.0
- Install: `pip install -r requirements.txt` or `docker compose up -build`

- **Experimental Grid**

- Fractions (regression: Concrete, Airfoil): $\{0.01, 0.05, 0.10, 0.25, 0.50\}$
- Fractions (classification: MNIST, CIFAR-10): $\{0.001, 0.002, 0.003, 0.005, 0.010\}$
- Seeds: 32 ($0 \dots 31$) with a fixed seeding routine.
- λ_0 grid: $\{1 \times 10^{-4}, 3 \times 10^{-4}, 1 \times 10^{-3}, 3 \times 10^{-3}, 1 \times 10^{-2}\}$
- Schedule exponent α : 1.0 (regression), 0.5 (classification)
- Optimizers: Adam ($lr = 10^{-3}$) and SGD+Momentum (regression $lr = 0.02$, classification $lr = 0.05$, momentum 0.9)
- Trust-region radii B : $\{5, 5\}$ (regression), $\{10, 10\}$ (classification)

- **Ablation Settings** We expose ablations via `-ablate: no_trust_region, no_grad_clip, 12` (use $L = L_{\text{data}} + \lambda \sum \|W\|^2$), and `constant_lambda` (use $\lambda(n) = \lambda_0$).

```
# examples
python -m src.ar.run --config configs/cifar10_cls.yaml --ablate no_trust_region
python -m src.ar.run --config configs/airfoil_reg.yaml --ablate 12,constant_lambda
```

We also provide lightweight ablation configs under `configs/ablation/` and (optionally) store ablation CSVs under `results/ablation/`.

- **Outputs** Each run writes (i) a per-run folder under `experiments/` containing configs, metrics, and diagnostics; and (ii) one row to a unified CSV. We provide four CSVs with a fixed header: `results_concrete_AR.csv`, `results_airfoil_AR.csv`, `results_mnist_AR.csv`, `results_cifar10_AR.csv`.

- **Results Artifacts** All table values are computed from the CSVs committed under `results/`: `results_concrete_AR.csv`, `results_airfoil_AR.csv`, `results_mnist_AR.csv`, and `results_cifar10_AR.csv`. To reproduce and verify:

```
python -m src.ar.run --config configs/concrete_reg.yaml
python -m src.ar.run --config configs/airfoil_reg.yaml
python -m src.ar.run --config configs/mnist_cls.yaml
python -m src.ar.run --config configs/cifar10_cls.yaml
```

and compare per-run rows with the provided CSVs (agreement within ± 0.001 for the reported metrics).

- **Continuous Integration** GitHub Actions runs unit tests and Fast CI configuration checks on every push/PR (dataset loaders, CSV schema, and ablation config parsing). A branch-protection rule requires the CI check to pass before merge.

- **Expected Agreement** Fixing the provided seeds reproduces all table values within ± 0.001 (accuracy, RMSE, ECE, etc.).

All components—code, data loaders, models, metrics, and logging—are public and version-pinned, ensuring end-to-end reproducibility on any standard CPU/GPU machine.

References

- [1] Organisation for Economic Co-operation and Development. Sme digitalisation to manage shocks and transitions: 2024 OECD D4SME survey. *OECD SME and Entrepreneurship Papers* No. 62, OECD Publishing, Paris, 2024.
- [2] S. Kergroach and J. Héritier. Emerging divides in the transition to artificial intelligence. *OECD Regional Development Papers* No. 147, OECD Publishing, Paris, 2025.
- [3] Giovanni Sartor and Francesca Lagioia. The impact of the general data protection regulation (gdpr) on artificial intelligence. *Study; Scientific Foresight Unit (STOA) PE 641.530*, European Parliamentary Research Service (EPRS), Brussels, 2020.
- [4] Songsong Tian, Lusi Li, Weijun Li, Hang Ran, Xin Ning, and Prayag Tiwari. A survey on few-shot class-incremental learning. *Neural Networks*, 169:307–324, 2024.

[5] Xian Tao, Xinyi Gong, Xin Zhang, Shaohua Yan, and Chandranath Adak. Deep learning for unsupervised anomaly localization in industrial images: A survey. *IEEE Transactions on Instrumentation and Measurement*, 71:1–21, 2022.

[6] Zaitian Wang, Pengfei Wang, Kunpeng Liu, Pengyang Wang, Yanjie Fu, Chang-Tien Lu, Charu C Aggarwal, Jian Pei, and Yuanchun Zhou. A comprehensive survey on data augmentation. *arXiv preprint arXiv:2405.09591*, 2024.

[7] Robert Geirhos, Jörn-Henrik Jacobsen, Claudio Michaelis, Richard Zemel, Wieland Brendel, Matthias Bethge, and Felix A Wichmann. Shortcut learning in deep neural networks. *Nature Machine Intelligence*, 2(11):665–673, 2020.

[8] Alexander Brown, Nenad Tomasev, Jan Freyberg, Yuan Liu, Alan Karthikesalingam, and Jessica Schrouff. Detecting shortcut learning for fair medical ai using shortcut testing. *Nature communications*, 14(1):4314, 2023.

[9] Trevor Hastie, Robert Tibshirani, Jerome Friedman, et al. The elements of statistical learning, 2009.

[10] Mikhail Belkin, Daniel Hsu, Siyuan Ma, and Soumik Mandal. Reconciling modern machine-learning practice and the classical bias–variance trade-off. *Proceedings of the National Academy of Sciences*, 116(32):15849–15854, 2019.

[11] Andrei Paleyes, Raoul-Gabriel Urma, and Neil D Lawrence. Challenges in deploying machine learning: a survey of case studies. *ACM computing surveys*, 55(6):1–29, 2022.

[12] David Sculley, Gary Holt, Daniel Golovin, Eugene Davydov, Todd Phillips, Dietmar Ebner, Vinay Chaudhary, Michael Young, Jean-Francois Crespo, and Dan Dennison. Hidden technical debt in machine learning systems. *Advances in neural information processing systems*, 28, 2015.

[13] Matthias De Lange, Rahaf Aljundi, Marc Masana, Sarah Parisot, Xu Jia, Aleš Leonardis, Gregory Slabaugh, and Tinne Tuytelaars. A continual learning survey: Defying forgetting in classification tasks. *IEEE transactions on pattern analysis and machine intelligence*, 44(7):3366–3385, 2021.

[14] John Schulman, Sergey Levine, Pieter Abbeel, Michael Jordan, and Philipp Moritz. Trust region policy optimization. In *International conference on machine learning*, pages 1889–1897. PMLR, 2015.

[15] Corinna Cortes and Vladimir Vapnik. Support-vector networks. *Machine learning*, 20(3):273–297, 1995.

[16] Chiyuan Zhang, Samy Bengio, Moritz Hardt, Benjamin Recht, and Oriol Vinyals. Understanding deep learning requires rethinking generalization. In *International Conference on Learning Representations*, 2017.

[17] Daniel Soudry, Elad Hoffer, Mor Shpigel Nacson, Suriya Gunasekar, and Nathan Srebro. The implicit bias of gradient descent on separable data. *Journal of Machine Learning Research*, 19(70):1–57, 2018.

[18] Peter L Bartlett, Philip M Long, Gábor Lugosi, and Alexander Tsigler. Benign overfitting in linear regression. *Proceedings of the National Academy of Sciences*, 117(48):30063–30070, 2020.

[19] Marco Loog, Tom Viering, Alexander Mey, Jesse H Krijthe, and David MJ Tax. A brief prehistory of double descent. *Proceedings of the National Academy of Sciences*, 117(20):10625–10626, 2020.

[20] Preetum Nakkiran, Gal Kaplun, Yamini Bansal, Tristan Yang, Boaz Barak, and Ilya Sutskever. Deep double descent: Where bigger models and more data hurt. *Journal of Statistical Mechanics: Theory and Experiment*, 2021(12):124003, 2021.

[21] Ben Adlam and Jeffrey Pennington. Understanding double descent requires a fine-grained bias-variance decomposition. *Advances in neural information processing systems*, 33:11022–11032, 2020.

[22] Trevor Hastie, Andrea Montanari, Saharon Rosset, and Ryan J Tibshirani. Surprises in high-dimensional ridgeless least squares interpolation. *Annals of statistics*, 50(2):949, 2022.

[23] Mikhail Belkin, Daniel Hsu, and Ji Xu. Two models of double descent for weak features. *SIAM Journal on Mathematics of Data Science*, 2(4), 2020.

[24] Vidya Muthukumar, Kailas Vodrahalli, Vignesh Subramanian, and Anant Sahai. Harmless interpolation of noisy data in regression. *IEEE Journal on Selected Areas in Information Theory*, 1(1):67–83, 2020.

[25] Mario Geiger, Stefano Spigler, Stéphane d’Ascoli, Levent Sagun, Marco Baity-Jesi, Giulio Biroli, and Matthieu Wyart. Jamming transition as a paradigm to understand the loss landscape of deep neural networks. *Physical Review E*, 100(1):012115, 2019.

[26] Stefano Spigler, Mario Geiger, Stéphane d’Ascoli, Levent Sagun, Giulio Biroli, and Matthieu Wyart. A jamming transition from under-to over-parametrization affects generalization in deep learning. *Journal of Physics A: Mathematical and Theoretical*, 52(47):474001, 2019.

[27] Madhu S Advani, Andrew M Saxe, and Haim Sompolinsky. High-dimensional dynamics of generalization error in neural networks. *Neural Networks*, 132:428–446, 2020.

- [28] Preetum Nakkiran, Prayaag Venkat, Sham Kakade, and Tengyu Ma. Optimal regularization can mitigate double descent. *arXiv preprint arXiv:2003.01897*, 2020.
- [29] Gabriel Pereyra, George Tucker, Jan Chorowski, Łukasz Kaiser, and Geoffrey Hinton. Regularizing neural networks by penalizing confident output distributions. *arXiv preprint arXiv:1701.06548*, 2017.
- [30] Christian Szegedy, Vincent Vanhoucke, Sergey Ioffe, Jon Shlens, and Zbigniew Wojna. Rethinking the inception architecture for computer vision. In *Proceedings of the IEEE conference on computer vision and pattern recognition*, pages 2818–2826, 2016.
- [31] Rafael Müller, Simon Kornblith, and Geoffrey E Hinton. When does label smoothing help? *Advances in neural information processing systems*, 32, 2019.
- [32] Youngdong Kim, Junho Yim, Juseung Yun, and Junmo Kim. Nlnl: Negative learning for noisy labels. In *Proceedings of the IEEE/CVF international conference on computer vision*, pages 101–110, 2019.
- [33] Takashi Ishida, Gang Niu, Weihua Hu, and Masashi Sugiyama. Learning from complementary labels. *Advances in neural information processing systems*, 30, 2017.
- [34] Marc’Aurelio Ranzato, Sumit Chopra, Michael Auli, and Wojciech Zaremba. Sequence level training with recurrent neural networks. In *4th International Conference on Learning Representations, ICLR 2016*, 2016.
- [35] Mohammad Norouzi, Samy Bengio, Navdeep Jaitly, Mike Schuster, Yonghui Wu, Dale Schuurmans, et al. Reward augmented maximum likelihood for neural structured prediction. *Advances In Neural Information Processing Systems*, 29, 2016.
- [36] Paul F Christiano, Jan Leike, Tom Brown, Miljan Martic, Shane Legg, and Dario Amodei. Deep reinforcement learning from human preferences. *Advances in neural information processing systems*, 30, 2017.
- [37] Daniel M Ziegler, Nisan Stiennon, Jeffrey Wu, Tom B Brown, Alec Radford, Dario Amodei, Paul Christiano, and Geoffrey Irving. Fine-tuning language models from human preferences, 2020. URL <https://arxiv.org/abs/>, page 14, 1909.
- [38] Long Ouyang, Jeffrey Wu, Xu Jiang, Diogo Almeida, Carroll Wainwright, Pamela Mishkin, Chong Zhang, Sandhini Agarwal, Katarina Slama, Alex Ray, et al. Training language models to follow instructions with human feedback. *Advances in neural information processing systems*, 35:27730–27744, 2022.
- [39] Rafael Rafailov, Archit Sharma, Eric Mitchell, Christopher D Manning, Stefano Ermon, and Chelsea Finn. Direct preference optimization: Your language model is secretly a reward model. *Advances in neural information processing systems*, 36:53728–53741, 2023.
- [40] Aaron van den Oord, Yazhe Li, and Oriol Vinyals. Representation learning with contrastive predictive coding. *arXiv preprint arXiv:1807.03748*, 2018.
- [41] Yaroslav Ganin, Evgeniya Ustinova, Hana Ajakan, Pascal Germain, Hugo Larochelle, François Laviolette, Mario March, and Victor Lempitsky. Domain-adversarial training of neural networks. *Journal of machine learning research*, 17(59):1–35, 2016.
- [42] Brian Hu Zhang, Blake Lemoine, and Margaret Mitchell. Mitigating unwanted biases with adversarial learning. In *Proceedings of the 2018 AAAI/ACM Conference on AI, Ethics, and Society*, pages 335–340, 2018.
- [43] Tuomas Haarnoja, Aurick Zhou, Pieter Abbeel, and Sergey Levine. Soft actor-critic: Off-policy maximum entropy deep reinforcement learning with a stochastic actor. In *International conference on machine learning*, pages 1861–1870. Pmlr, 2018.
- [44] Hirotugu Akaike. A new look at the statistical model identification. *IEEE transactions on automatic control*, 19(6):716–723, 2003.
- [45] MALLOWS CL. Some comments on c_p. *Technometrics*, 15:661–675, 1973.
- [46] Charles M Stein. Estimation of the mean of a multivariate normal distribution. *The annals of Statistics*, pages 1135–1151, 1981.
- [47] Peter Craven and Grace Wahba. Smoothing noisy data with spline functions: estimating the correct degree of smoothing by the method of generalized cross-validation. *Numerische mathematik*, 31(4):377–403, 1978.
- [48] Grace Wahba. *Spline models for observational data*. SIAM, 1990.
- [49] Jianming Ye. On measuring and correcting the effects of data mining and model selection. *Journal of the American Statistical Association*, 93(441):120–131, 1998.
- [50] Bradley Efron, Trevor Hastie, Iain Johnstone, and Robert Tibshirani. Least angle regression. *Annals of Statistics*, pages 407–451, 2004.

- [51] HUI ZOU, Trevor HASTIE, and Robert TIBSHIRANI. On the degrees of freedom of the lasso. *Annals of statistics*, 35(5):2173–2192, 2007.
- [52] RYAN J TIBSHIRANI and JONATHAN TAYLOR. Degrees of freedom in lasso problems. *The Annals of Statistics*, 40(2):1198–1232, 2012.
- [53] David L Donoho and Iain M Johnstone. Adapting to unknown smoothness via wavelet shrinkage. *Journal of the american statistical association*, 90(432):1200–1224, 1995.
- [54] Mervyn Stone. Cross-validatory choice and assessment of statistical predictions. *Journal of the royal statistical society: Series B (Methodological)*, 36(2):111–133, 1974.
- [55] Lutz Prechelt. Early stopping-but when? In *Neural Networks: Tricks of the trade*, pages 55–69. Springer, 2002.
- [56] Yuan Yao, Lorenzo Rosasco, and Andrea Caponnetto. On early stopping in gradient descent learning. *Constructive approximation*, 26(2):289–315, 2007.
- [57] Garvesh Raskutti, Martin J Wainwright, and Bin Yu. Early stopping and non-parametric regression: an optimal data-dependent stopping rule. *The Journal of Machine Learning Research*, 15(1):335–366, 2014.
- [58] Stephan Mandt, Matthew D Hoffman, and David M Blei. Stochastic gradient descent as approximate bayesian inference. *Journal of Machine Learning Research*, 18(134):1–35, 2017.
- [59] Samuel L Smith and Quoc V Le. A bayesian perspective on generalization and stochastic gradient descent. In *International Conference on Learning Representations*, 2018.
- [60] Stanisław Jastrzębski, Zachary Kenton, Devansh Arpit, Nicolas Ballas, Asja Fischer, Yoshua Bengio, and Amos Storkey. Three factors influencing minima in sgd. *arXiv preprint arXiv:1711.04623*, 2017.
- [61] Nitish Shirish Keskar, Dheevatsa Mudigere, Jorge Nocedal, Mikhail Smelyanskiy, and Ping Tak Peter Tang. On large-batch training for deep learning: Generalization gap and sharp minima. In *International Conference on Learning Representations*, 2017.
- [62] Ilya Loshchilov and Frank Hutter. Decoupled weight decay regularization. *arXiv preprint arXiv:1711.05101*, 2017.
- [63] Leslie N Smith. Cyclical learning rates for training neural networks. In *2017 IEEE winter conference on applications of computer vision (WACV)*, pages 464–472. IEEE, 2017.
- [64] Olivier Bousquet and André Elisseeff. Stability and generalization. *Journal of machine learning research*, 2(Mar):499–526, 2002.
- [65] Moritz Hardt, Ben Recht, and Yoram Singer. Train faster, generalize better: Stability of stochastic gradient descent. In *International conference on machine learning*, pages 1225–1234. PMLR, 2016.
- [66] Chuan Guo, Geoff Pleiss, Yu Sun, and Kilian Q Weinberger. On calibration of modern neural networks. In *International conference on machine learning*, pages 1321–1330. PMLR, 2017.
- [67] Giorgio Patrini, Alessandro Rozza, Aditya Krishna Menon, Richard Nock, and Lizhen Qu. Making deep neural networks robust to label noise: A loss correction approach. In *Proceedings of the IEEE conference on computer vision and pattern recognition*, pages 1944–1952, 2017.
- [68] Aritra Ghosh, Himanshu Kumar, and P Shanti Sastry. Robust loss functions under label noise for deep neural networks. In *Proceedings of the AAAI conference on artificial intelligence*, volume 31, 2017.
- [69] Zhilu Zhang and Mert Sabuncu. Generalized cross entropy loss for training deep neural networks with noisy labels. *Advances in neural information processing systems*, 31, 2018.
- [70] Yisen Wang, Xingjun Ma, Zaiyi Chen, Yuan Luo, Jinfeng Yi, and James Bailey. Symmetric cross entropy for robust learning with noisy labels. In *Proceedings of the IEEE/CVF international conference on computer vision*, pages 322–330, 2019.
- [71] Takeru Miyato, Shin-ichi Maeda, Masanori Koyama, and Shin Ishii. Virtual adversarial training: a regularization method for supervised and semi-supervised learning. *IEEE transactions on pattern analysis and machine intelligence*, 41(8):1979–1993, 2018.
- [72] Hongyi Zhang, Moustapha Cisse, Yann N Dauphin, and David Lopez-Paz. mixup: Beyond empirical risk minimization. In *International Conference on Learning Representations*, 2018.
- [73] Sunil Thulasidasan, Gopinath Chennupati, Jeff A Bilmes, Tanmoy Bhattacharya, and Sarah Michalak. On mixup training: Improved calibration and predictive uncertainty for deep neural networks. *Advances in neural information processing systems*, 32, 2019.

[74] Razvan Pascanu, Tomas Mikolov, and Yoshua Bengio. On the difficulty of training recurrent neural networks. In *International conference on machine learning*, pages 1310–1318. Pmlr, 2013.

[75] Aleksander Madry, Aleksandar Makelov, Ludwig Schmidt, Dimitris Tsipras, and Adrian Vladu. Towards deep learning models resistant to adversarial attacks. In *International Conference on Learning Representations*, 2018.

[76] Hongyang Zhang, Yaodong Yu, Jiantao Jiao, Eric Xing, Laurent El Ghaoui, and Michael Jordan. Theoretically principled trade-off between robustness and accuracy. In *International conference on machine learning*, pages 7472–7482. PMLR, 2019.

[77] Moustapha Cisse, Piotr Bojanowski, Edouard Grave, Yann Dauphin, and Nicolas Usunier. Parseval networks: Improving robustness to adversarial examples. In *International conference on machine learning*, pages 854–863. PMLR, 2017.

[78] Jeremy Cohen, Elan Rosenfeld, and Zico Kolter. Certified adversarial robustness via randomized smoothing. In *international conference on machine learning*, pages 1310–1320. PMLR, 2019.

[79] Arthur Jacot, Franck Gabriel, and Clément Hongler. Neural tangent kernel: Convergence and generalization in neural networks. *Advances in neural information processing systems*, 31, 2018.

[80] Jaehoon Lee, Lechao Xiao, Samuel Schoenholz, Yasaman Bahri, Roman Novak, Jascha Sohl-Dickstein, and Jeffrey Pennington. Wide neural networks of any depth evolve as linear models under gradient descent. *Advances in neural information processing systems*, 32, 2019.

[81] Lenaic Chizat, Edouard Oyallon, and Francis Bach. On lazy training in differentiable programming. *Advances in neural information processing systems*, 32, 2019.

[82] Simon Du, Jason Lee, Haochuan Li, Liwei Wang, and Xiyu Zhai. Gradient descent finds global minima of deep neural networks. In *International conference on machine learning*, pages 1675–1685. PMLR, 2019.

[83] Blake Bordelon, Abdulkadir Canatar, and Cengiz Pehlevan. Spectrum dependent learning curves in kernel regression and wide neural networks. In *International Conference on Machine Learning*, pages 1024–1034. PMLR, 2020.

[84] Abdulkadir Canatar, Blake Bordelon, and Cengiz Pehlevan. Spectral bias and task-model alignment explain generalization in kernel regression and infinitely wide neural networks. *Nature communications*, 12(1):2914, 2021.

[85] T Liang and A Rakhlin. Just interpolate: Kernel “ridgeless” regression can generalize. 757 arxiv e-prints p. *arXiv preprint arXiv:1808.00387*, 758, 2018.

[86] Song Mei and Andrea Montanari. The generalization error of random features regression: Precise asymptotics and the double descent curve. *Communications on Pure and Applied Mathematics*, 75(4):667–766, 2022.

[87] Ali Rahimi and Benjamin Recht. Random features for large-scale kernel machines. *Advances in neural information processing systems*, 20, 2007.

[88] Alessandro Rudi and Lorenzo Rosasco. Generalization properties of learning with random features. *Advances in neural information processing systems*, 30, 2017.

[89] Nasim Rahaman, Aristide Baratin, Devansh Arpit, Felix Draxler, Min Lin, Fred Hamprecht, Yoshua Bengio, and Aaron Courville. On the spectral bias of neural networks. In *International conference on machine learning*, pages 5301–5310. PMLR, 2019.

[90] Arthur E Hoerl and Robert W Kennard. Ridge regression: Biased estimation for nonorthogonal problems. *Technometrics*, 12(1):55–67, 1970.

[91] Heinz W Engl and Ronny Ramlau. Regularization of inverse problems. In *Encyclopedia of applied and computational mathematics*, pages 1233–1241. Springer, 2015.

[92] Per Christian Hansen. *Discrete inverse problems: insight and algorithms*. SIAM, 2010.

A Preliminaries and Notation

A.1 Notation Summary

Throughout this appendix, we assume a fixed design where the sample size is denoted by $n := |S|$. Unless otherwise specified, expectations $\mathbb{E}[\cdot]$ are taken with respect to the noise variable ε , conditional on the inputs.

Assumptions of the Regression Model We assume the model $y = X\theta^* + \varepsilon$, where $\varepsilon \sim (0, \tau^2 I)$. The estimator is expressed via the linear smoother as $\hat{f}_\lambda = S_\lambda y$.

Table 15: Summary of Notation

Symbol	Meaning	Shape/Domain
$S = \{(x_i, y_i)\}_{i=1}^n$	Training dataset	$x_i \in \mathbb{R}^p, y_i \in \mathbb{R}$ or $\{1, \dots, C\}$
$X = [x_1^\top; \dots; x_n^\top]$	Design matrix	$\mathbb{R}^{n \times p}$
$y = (y_1, \dots, y_n)^\top$	Response vector	\mathbb{R}^n
θ	Parameter vector (or network weights)	\mathbb{R}^p or multi-tensor
$f_\theta(\cdot)$	Prediction function	$\mathbb{R}^p \rightarrow \mathbb{R}$ or Δ^{C-1}
$\ell(\theta; x, y)$	Loss function	Reg: squared loss; Cls: cross-entropy
$\hat{F}_\lambda(\theta)$	Regularized empirical risk objective	$\frac{1}{n} \sum \ell(\theta; x_i, y_i) - \lambda R(\theta)$
λ	Anti-regularization coefficient (reward strength)	$\lambda \geq 0$
$R(\theta)$	Regularization/reward term	$\frac{1}{2} \ \theta\ _2^2$ or $\frac{1}{2} \theta^\top W \theta$
$W \succeq 0$	Spectrum-weighting matrix	$\mathbb{R}^{p \times p}$
$\hat{\Sigma} = \frac{1}{n} X^\top X$	Sample covariance (fixed design)	$\mathbb{R}^{p \times p}$
$\sigma_{\min / \max}(A)$	Minimum/maximum eigenvalue of symmetric A	$\mathbb{R}_{\geq 0}$
S_λ	Linear smoother	$X(X^\top X - n\lambda I)^{-1} X^\top \in \mathbb{R}^{n \times n}$
$\text{df}(\lambda)$	Degrees of freedom	$\text{tr}(S_\lambda)$
ε	Noise	$\mathbb{E}[\varepsilon] = 0, \text{Var}(\varepsilon) = \tau^2 I$
τ^2	Noise variance (homoskedastic)	$\mathbb{R}_{>0}$
$H(p_y, q_\theta(x))$	Classification loss (CE)	p_y : one-hot, q_θ : predicted distribution
$m_\theta(x, y)$	Margin	Defined per problem via logit differences, etc.
ϕ	Bounded Lipschitz reward function	Bounded and Lipschitz
G	Network Lipschitz constant	$\mathbb{R}_{>0}$
K	NTK/kernel matrix	$\mathbb{R}^{n \times n}$
$\ \cdot\ _{\mathcal{H}_K}$	RKHS norm	Induced by kernel K

Definition of Empirical and Test Risk We consistently adopt the following definitions throughout the paper:

$$\widehat{\mathcal{R}}_S(\hat{f}_\lambda) := \frac{1}{n} \|y - \hat{f}_\lambda\|_2^2 - \tau^2, \quad \mathcal{R}(\hat{f}_\lambda) := \frac{1}{n} \mathbb{E}_{\varepsilon'} [\|y^{\text{new}} - \hat{f}_\lambda\|_2^2],$$

where $y^{\text{new}} = X\theta^* + \varepsilon'$, $\varepsilon' \stackrel{\text{i.i.d.}}{\sim} (0, \tau^2 I)$, and $\varepsilon' \perp\!\!\!\perp \varepsilon$. Under these definitions, the optimism identity holds as

$$\mathbb{E}[\mathcal{R}] = \mathbb{E}[\widehat{\mathcal{R}}_S] + \frac{2\tau^2}{n} \text{tr}(S_\lambda).$$

For a detailed derivation, see Section A.3.

A.2 Basic Spectral Facts

This subsection collects standard facts repeatedly used in the subsequent proofs. Unless stated otherwise, all matrices are assumed to be real and symmetric.

Lemma 8 (Spectral Bounds and Quadratic Forms). *For symmetric $A \succeq 0$ and any vector v ,*

$$\sigma_{\min}(A) \|v\|_2^2 \leq v^\top A v \leq \sigma_{\max}(A) \|v\|_2^2.$$

Also, if $\lambda < \sigma_{\min}(A)$, then $\|(A - \lambda I)^{-1}\|_2 = \frac{1}{\sigma_{\min}(A) - \lambda}$.

Lemma 9 (Trace Monotonicity and Differentiation). *Given the eigendecomposition $A = U \text{diag}(\sigma_j) U^\top$ and scalar λ ,*

$$\text{tr}(A(A - \lambda I)^{-1}) = \sum_j \frac{\sigma_j}{\sigma_j - \lambda}, \quad \frac{\partial}{\partial \lambda} \text{tr}(A(A - \lambda I)^{-1}) = \sum_j \frac{\sigma_j}{(\sigma_j - \lambda)^2} > 0.$$

More generally, for invertible $M(\lambda)$,

$$\frac{\partial}{\partial \lambda} M^{-1} = -M^{-1} \left(\frac{\partial M}{\partial \lambda} \right) M^{-1}.$$

Lemma 10 (PSD Ordering and Trace). *If $0 \preceq B \preceq C$ and $M \succeq 0$, then $\text{tr}(MB) \leq \text{tr}(MC)$.*

Lemma 11 (Sherman–Morrison–Woodbury Formula). *For invertible A and compatible dimensions of U, C, V ,*

$$(A + UCV)^{-1} = A^{-1} - A^{-1}U(C^{-1} + VA^{-1}U)^{-1}VA^{-1}.$$

This is especially useful when $A = X^\top X - n\lambda I$, enabling efficient updates of A^{-1} .

Lemma 12 (Weyl's Inequality (Simplified)). *For symmetric A, B ,*

$$\sigma_{\min}(A) + \sigma_{\min}(B) \leq \sigma_{\min}(A + B) \leq \sigma_{\max}(A + B) \leq \sigma_{\max}(A) + \sigma_{\max}(B).$$

Remark 1 (Spectral Expression for Degrees of Freedom). *If $\hat{\Sigma} = U \text{diag}(\sigma_j)U^\top$, then*

$$\text{tr}(S_\lambda) = \sum_j \frac{\sigma_j}{\sigma_j - \lambda},$$

which is strictly increasing in λ whenever $\lambda < \sigma_{\min}(\hat{\Sigma})$.

A.3 Optimism Identity Background

This section summarizes the derivation of the following identity under the linear smoother $\hat{f}_\lambda = S_\lambda y$:

$$\mathbb{E}[\mathcal{R}(\hat{f}_\lambda)] = \mathbb{E}[\hat{\mathcal{R}}_S(\hat{f}_\lambda)] + \frac{2\tau^2}{n} \text{tr}(S_\lambda),$$

which belongs to the same family of results as Stein's Unbiased Risk Estimate (SURE) and the optimism identity in prediction.

Lemma 13 (Optimism Identity). *Assume the generative model $y = X\theta^* + \varepsilon$, where $\varepsilon \sim (0, \tau^2 I)$, and define the smoother $\hat{f}_\lambda = S_\lambda y$. Using the definitions of $\hat{\mathcal{R}}_S$ and \mathcal{R} from §A.1, we have*

$$\mathbb{E}[\mathcal{R}(\hat{f}_\lambda)] = \mathbb{E}[\hat{\mathcal{R}}_S(\hat{f}_\lambda)] + \frac{2\tau^2}{n} \text{tr}(S_\lambda).$$

Proof sketch. Start from the decomposition: $\hat{f}_\lambda = S_\lambda(X\theta^* + \varepsilon) = S_\lambda X\theta^* + S_\lambda \varepsilon$. For new responses $y^{\text{new}} = X\theta^* + \varepsilon'$, we compute

$$\frac{1}{n} \mathbb{E}_{\varepsilon'} [\|y^{\text{new}} - \hat{f}_\lambda\|^2] = \frac{1}{n} \|X\theta^* - \hat{f}_\lambda\|^2 + \tau^2.$$

On the other hand,

$$\frac{1}{n} \|y - \hat{f}_\lambda\|^2 = \frac{1}{n} \|X\theta^* - \hat{f}_\lambda\|^2 + \frac{2}{n} \varepsilon^\top (I - S_\lambda)(X\theta^* - \hat{f}_\lambda) + \frac{1}{n} \|(I - S_\lambda)\varepsilon\|^2.$$

Taking expectation over ε , the cross term vanishes, and the last term becomes

$$\frac{1}{n} \mathbb{E}[\text{tr}((I - S_\lambda)^2 \varepsilon \varepsilon^\top)] = \frac{\tau^2}{n} \text{tr}((I - S_\lambda)^2).$$

By definition, $\hat{\mathcal{R}}_S = \frac{1}{n} \|y - \hat{f}_\lambda\|^2 - \tau^2$, so we obtain

$$\mathbb{E}[\mathcal{R}] = \mathbb{E}[\hat{\mathcal{R}}_S] + \frac{\tau^2}{n} \{\text{tr}((I - S_\lambda)^2) - \text{tr}(I)\}.$$

For linear smoothers, the identity $\text{tr}((I - S_\lambda)^2) - \text{tr}(I) = -2 \text{tr}(S_\lambda)$ holds, which completes the proof. \square

Remark 2 (Degrees of Freedom Interpretation). *In the above identity, $\text{tr}(S_\lambda)$ acts as the model degrees of freedom. Thus, strategies that control $\text{tr}(S_\lambda)$ to remain constant or decay with sample size offer a principled way to manage the bias–variance tradeoff.*

B Regression: Unique Convergence in the Safe Zone

B.1 Proof of Strong Convexity

Theorem 14 (Safe Region and Strong Convexity in Regression). *Let the design matrix be $X \in \mathbb{R}^{n \times p}$ and $\hat{\Sigma} = \frac{1}{n} X^\top X$. For the regression loss $\ell(\theta; x, y) = \frac{1}{2}(y - x^\top \theta)^2$ and reward $R(\theta) = \frac{1}{2}\|\theta\|_2^2$, the objective*

$$\hat{F}_\lambda(\theta) = \frac{1}{n} \sum_{i=1}^n \frac{1}{2}(y_i - x_i^\top \theta)^2 - \frac{\lambda}{2}\|\theta\|_2^2$$

has Hessian $H_\lambda = \hat{\Sigma} - \lambda I$. If $\lambda < \sigma_{\min}(\hat{\Sigma})$, then $H_\lambda \succ 0$, which implies \hat{F}_λ is μ -strongly convex with $\mu = \sigma_{\min}(\hat{\Sigma}) - \lambda > 0$, and the global minimizer is unique.

Proof. We compute $\nabla^2 \hat{F}_\lambda = \hat{\Sigma} - \lambda I$. By spectral bounds of symmetric matrices, we have $\sigma_{\min}(H_\lambda) = \sigma_{\min}(\hat{\Sigma}) - \lambda$. By assumption, this quantity is positive, i.e., $H_\lambda \succ 0$, so \hat{F}_λ is μ -strongly convex and has a unique minimizer. \square

Remark 3 (Tightness of the Boundary). *If $\lambda \geq \sigma_{\min}(\hat{\Sigma})$, then H_λ becomes semi-definite or indefinite, breaking strong convexity. In particular, when $\lambda > \sigma_{\min}(\hat{\Sigma})$, there exists a direction of negative curvature, and the objective can become unbounded below. Specifically, let u be a unit eigenvector of $\hat{\Sigma}$ such that $\hat{\Sigma}u = \sigma_{\min}(\hat{\Sigma})u$, then for $\theta = tu$,*

$$\hat{F}_\lambda(tu) = \frac{1}{2}t^2(\sigma_{\min}(\hat{\Sigma}) - \lambda) - \frac{t}{n}y^\top Xu + \text{const},$$

and the coefficient of t^2 is negative, so $\hat{F}_\lambda(tu) \rightarrow -\infty$ as $t \rightarrow \infty$.

Remark 4 (Extension to Weighted Rewards). *If the reward term is generalized to $R(\theta) = \frac{1}{2}\theta^\top W\theta$ with $W \succeq 0$, then the Hessian becomes $H_\lambda = \hat{\Sigma} - \lambda W$. The safe condition is then given in terms of the generalized eigenvalue problem as $\lambda < \inf_{\|v\|=1} \frac{v^\top \hat{\Sigma} v}{v^\top W v}$. When $W = I$, this reduces to the original theorem.*

B.2 Closed-Form Solution and Gradient Descent Convergence

Corollary 15 (Closed-Form Solution). *Under the assumptions of the theorem, the first-order optimality condition $\nabla \hat{F}_\lambda(\theta) = 0$ becomes*

$$(\hat{\Sigma} - \lambda I)\hat{\theta}_\lambda = \frac{1}{n}X^\top y \iff \hat{\theta}_\lambda = (\hat{\Sigma} - \lambda I)^{-1}\frac{1}{n}X^\top y = (X^\top X - n\lambda I)^{-1}X^\top y.$$

The solution is unique and exists since $H_\lambda \succ 0$.

Proof. We compute $\nabla \hat{F}_\lambda(\theta) = \hat{\Sigma}\theta - \frac{1}{n}X^\top y - \lambda\theta$. Setting this to zero yields a linear equation, and since H_λ is invertible, the solution follows. \square

Theorem 16 (Linear Convergence of Gradient Descent). *Consider standard gradient descent on the objective \hat{F}_λ : $\theta_{t+1} = \theta_t - \eta \nabla \hat{F}_\lambda(\theta_t)$. Let $L = \sigma_{\max}(H_\lambda) = \sigma_{\max}(\hat{\Sigma}) - \lambda$, and $\mu = \sigma_{\min}(H_\lambda) = \sigma_{\min}(\hat{\Sigma}) - \lambda$. If $0 < \eta < \frac{2}{L}$, then*

$$\|\theta_t - \hat{\theta}_\lambda\|_2 \leq \rho^t \|\theta_0 - \hat{\theta}_\lambda\|_2, \quad \rho = \max_j |1 - \eta \sigma_j(H_\lambda)| < 1,$$

i.e., the convergence is linear. The optimal fixed step size is $\eta^ = \frac{2}{L+\mu}$, yielding rate $\rho^* = \frac{\kappa-1}{\kappa+1}$ with condition number $\kappa = \frac{L}{\mu}$.*

Proof. Since the objective is quadratic, the error $e_t = \theta_t - \hat{\theta}_\lambda$ evolves as $e_{t+1} = (I - \eta H_\lambda)e_t$, implying $\|e_{t+1}\|_2 \leq \|I - \eta H_\lambda\|_2 \|e_t\|_2$. By spectral decomposition, $\|I - \eta H_\lambda\|_2 = \max_j |1 - \eta \sigma_j(H_\lambda)|$. For $\eta \in (0, 2/L)$, this quantity is less than 1, guaranteeing linear convergence. The expressions for η^* and ρ^* follow from classical optimization theory. \square

Remark 5 (Step Size and Numerical Stability). *In practice, upper bounds on L are often overestimated, so a conservative step size such as $\eta \leq \frac{1}{L}$ is used, possibly with outer line search. When using a mini-batch variant, due to variance in H_λ , reducing η further is often advisable for stability.*

B.3 Comments and Counterexamples Near the Boundary

Condition Number Deterioration As $\lambda \uparrow \sigma_{\min}(\hat{\Sigma})$, the strong convexity constant $\mu = \sigma_{\min}(\hat{\Sigma}) - \lambda \downarrow 0$, causing the condition number $\kappa = \frac{L}{\mu}$ to explode. Consequently, the optimal convergence rate of GD $\rho^* = \frac{\kappa-1}{\kappa+1}$ approaches 1, and the closed-form solution becomes numerically unstable due to

$$\|(X^\top X - n\lambda I)^{-1}\|_2 = \frac{1}{n(\sigma_{\min}(\hat{\Sigma}) - \lambda)} \rightarrow \infty.$$

Practical Safeguards A safety margin $\epsilon \in (0, 1)$ is introduced to restrict $\lambda \leq (1 - \epsilon)\sigma_{\min}(\hat{\Sigma})$. The quantity $\sigma_{\min}(\hat{\Sigma})$ can be approximated via the power method or randomized SVD, using the lower bound of its confidence interval to avoid overestimation. If using weighted regularization $W \succeq 0$, one solves the generalized eigenvalue problem to estimate a lower bound on $\inf_{v \neq 0} \frac{v^\top \hat{\Sigma} v}{v^\top W v}$.

Explicit Counterexample Let $\hat{\Sigma} = \text{diag}(1, \delta)$, $0 < \delta < 1$, and $\lambda = \frac{1+\delta}{2}$. Then,

$$H_\lambda = \text{diag}\left(\frac{1-\delta}{2}, -\frac{1-\delta}{2}\right)$$

has a negative eigenvalue. Along the direction $u = (0, 1)^\top$, the objective $\hat{F}_\lambda(tu) \rightarrow -\infty$ as $t \rightarrow \infty$, implying the objective is unbounded below if λ exceeds the spectral bound.

Alternative Remedies Instability near the boundary can be mitigated through: (i) Reducing λ further or applying a decay schedule $|\lambda(n)| \propto n^{-\alpha}$ as sample size increases; (ii) Temporarily combining a trust region constraint $\|\theta\| \leq B$ to prevent numerical blow-up; (iii) Aligning the coordinate system $X = U\Sigma^{1/2}V^\top$ and selectively damping the small eigenspace directions.

C Degrees of Freedom and Test Risk Improvement

C.1 Spectral Derivation of Degrees of Freedom

Proposition 17 (Spectral Expression for Degrees of Freedom). *Let the eigenvalues of $\hat{\Sigma} = \frac{1}{n}X^\top X$ be $\{\sigma_j\}_{j=1}^r$, where $r = \text{rank}(X)$. Then, for the linear smoother*

$$S_\lambda = X(X^\top X - n\lambda I)^{-1}X^\top \in \mathbb{R}^{n \times n},$$

we have

$$\text{tr}(S_\lambda) = \sum_{j=1}^r \frac{\sigma_j}{\sigma_j - \lambda}, \quad \text{valid for } \lambda < \sigma_{\min}(\hat{\Sigma}).$$

Proof. Using the cyclic property of the trace:

$$\text{tr}(S_\lambda) = \text{tr}\left((X^\top X - n\lambda I)^{-1}X^\top X\right).$$

Given $\hat{\Sigma} = V \text{diag}(\sigma_j) V^\top$, we write $X^\top X = nV \text{diag}(\sigma_j) V^\top$, and thus:

$$(X^\top X - n\lambda I)^{-1} = (nV \text{diag}(\sigma_j - \lambda) V^\top)^{-1} = \frac{1}{n}V \text{diag}\left(\frac{1}{\sigma_j - \lambda}\right) V^\top.$$

So we get:

$$\text{tr}(S_\lambda) = \text{tr} \left(V \text{diag} \left(\frac{1}{\sigma_j - \lambda} \right) V^\top \cdot V \text{diag}(\sigma_j) V^\top \right) = \sum_{j=1}^r \frac{\sigma_j}{\sigma_j - \lambda}.$$

Eigenvalues that are zero do not contribute to the trace. \square

Remark 6 (Smoothing Coefficients). *With $X = U\Sigma^{1/2}V^\top$ and row-orthogonal U , the smoother becomes*

$$S_\lambda = U \text{diag} \left(\frac{\sigma_j}{\sigma_j - \lambda} \right) U^\top,$$

and each mode contributes a smoothing coefficient $h_j(\lambda) = \frac{\sigma_j}{\sigma_j - \lambda}$ to the total degrees of freedom.

C.2 Proof of Test Risk Improvement Theorem

Theorem 18 (Sufficient Condition for Test Risk Improvement — Restatement). *Let*

$$\widehat{\mathcal{R}}_S(\hat{f}) = \frac{1}{n} \|y - \hat{f}\|_2^2 - \tau^2, \quad \mathcal{R}(\hat{f}) = \frac{1}{n} \mathbb{E}_{\varepsilon'} \left[\|y^{new} - \hat{f}\|_2^2 \right],$$

and define

$$\Delta \widehat{\mathcal{R}}_S := \widehat{\mathcal{R}}_S(\hat{f}_0) - \widehat{\mathcal{R}}_S(\hat{f}_\lambda) \geq 0, \quad \Delta \text{tr} := \text{tr}(S_\lambda) - \text{tr}(S_0) \geq 0.$$

Then, from the optimism identity

$$\mathbb{E}[\mathcal{R}(\hat{f}_\lambda)] = \mathbb{E}[\widehat{\mathcal{R}}_S(\hat{f}_\lambda)] + \frac{2\tau^2}{n} \text{tr}(S_\lambda),$$

we obtain the implication:

$$\Delta \widehat{\mathcal{R}}_S > \frac{2\tau^2}{n} \Delta \text{tr} \implies \mathbb{E}[\mathcal{R}(\hat{f}_\lambda)] < \mathbb{E}[\mathcal{R}(\hat{f}_0)].$$

Proof. Subtract the test risks of the two models:

$$\mathbb{E}[\mathcal{R}(\hat{f}_\lambda) - \mathcal{R}(\hat{f}_0)] = \mathbb{E}[\widehat{\mathcal{R}}_S(\hat{f}_\lambda) - \widehat{\mathcal{R}}_S(\hat{f}_0)] + \frac{2\tau^2}{n} (\text{tr}(S_\lambda) - \text{tr}(S_0)).$$

The second term is $\frac{2\tau^2}{n} \Delta \text{tr}$, and the first is $-\Delta \widehat{\mathcal{R}}_S$. If $\Delta \widehat{\mathcal{R}}_S > \frac{2\tau^2}{n} \Delta \text{tr}$, their sum is negative. \square

Remark 7 (Boundary and Interpretation). *At equality, the two risks are the same; below that threshold, improvement occurs. The term $\frac{2\tau^2}{n} \text{tr}(S_\lambda)$ represents a variance penalty, so increasing the degrees of freedom too much via λ (near the safe boundary) can nullify the benefit.*

C.3 Monotonicity and Sensitivity Analysis

Proposition 19 (Monotonicity). *In the safe region $\lambda < \sigma_{\min}(\hat{\Sigma})$, we have*

$$\frac{\partial}{\partial \lambda} \text{tr}(S_\lambda) = \sum_{j=1}^r \frac{\sigma_j}{(\sigma_j - \lambda)^2} > 0,$$

so $\text{tr}(S_\lambda)$ is strictly increasing in λ .

Proof. We apply termwise differentiation to $\text{tr}(S_\lambda) = \sum_j \frac{\sigma_j}{\sigma_j - \lambda}$. \square

Corollary 20 (Lipschitz-Type Bounds). *Let $s_{\min} = \sigma_{\min}(\hat{\Sigma})$, $s_{\max} = \sigma_{\max}(\hat{\Sigma})$, and $r = \text{rank}(X)$. For any $\lambda_2 \geq \lambda_1$, the mean value theorem yields*

$$0 \leq \text{tr}(S_{\lambda_2}) - \text{tr}(S_{\lambda_1}) \leq (\lambda_2 - \lambda_1) \frac{rs_{\max}}{(s_{\min} - \lambda_2)^2}.$$

Moreover, each term satisfies

$$\frac{\sigma_j}{(\sigma_j - \lambda)^2} \geq \frac{s_{\min}}{(s_{\max} - \lambda)^2},$$

so

$$\frac{\partial}{\partial \lambda} \text{tr}(S_{\lambda}) \geq \frac{rs_{\min}}{(s_{\max} - \lambda)^2}.$$

Proposition 21 (Spectral Sensitivity). *The sensitivity of each term with respect to σ_j is given by*

$$\frac{\partial}{\partial \sigma_j} \left(\frac{\sigma_j}{\sigma_j - \lambda} \right) = -\frac{\lambda}{(\sigma_j - \lambda)^2} < 0.$$

Thus, the larger the small eigenvalues σ_j , the more suppressed the degree-of-freedom inflation; smaller σ_j lead to sharper increases in $\text{tr}(S_{\lambda})$.

Remark 8 (Practical Summary). *When many small σ_j exist, $\text{tr}(S_{\lambda})$ becomes steeper, leading to rapid growth of the variance penalty. Combining a safe slack margin $\lambda \leq (1 - \epsilon)s_{\min}$ with a sample-size-based schedule $|\lambda(n)| \propto n^{-\alpha}$ helps keep the degrees of freedom per sample under control.*

D Sample Size Scaling Rule (Regression)

D.1 Degree-of-Freedom Targeting Rule

We aim to maintain a fixed complexity per sample by solving

$$\frac{1}{n} \text{tr}(S_{\lambda}) = \kappa \iff \text{tr}(S_{\lambda}) = \kappa n,$$

for λ , where $S_{\lambda} = X(X^{\top}X - n\lambda I)^{-1}X^{\top}$, and the eigenvalues of $\hat{\Sigma} = \frac{1}{n}X^{\top}X$ are denoted $\{\sigma_j\}_{j=1}^r$.

Proposition 22 (Existence and Uniqueness). *In the safe region $\lambda < \sigma_{\min}(\hat{\Sigma})$, we have*

$$\text{tr}(S_{\lambda}) = \sum_{j=1}^r \frac{\sigma_j}{\sigma_j - \lambda},$$

which is continuous and strictly increasing in λ . Moreover, $\text{tr}(S_0) = r$ and $\lim_{\lambda \uparrow \sigma_{\min}(\hat{\Sigma})} \text{tr}(S_{\lambda}) = +\infty$. Therefore, for any $\kappa > \frac{r}{n}$, the equation $\text{tr}(S_{\lambda}) = \kappa n$ has a unique solution.

Proof sketch. Using spectral decomposition and termwise differentiation, $\frac{d}{d\lambda} \text{tr}(S_{\lambda}) = \sum_j \frac{\sigma_j}{(\sigma_j - \lambda)^2} > 0$, so monotonicity holds. Divergence at $\lambda \rightarrow \sigma_{\min}^-(\hat{\Sigma})$ guarantees the intermediate value theorem applies. \square

First-order Approximation for Small λ When λ is small,

$$\text{tr}(S_{\lambda}) = \sum_{j=1}^r \left(1 + \frac{\lambda}{\sigma_j} + O(\lambda^2) \right) = r + \lambda \sum_{j=1}^r \frac{1}{\sigma_j} + O(\lambda^2).$$

Thus, an initial guess for λ is given by

$$\lambda^{(0)} \approx \frac{\kappa n - r}{\sum_{j=1}^r \frac{1}{\sigma_j}} \quad (\text{valid if } > 0).$$

Numerical Solution (Monotonic Equation) Bisection within $\lambda \in [0, (1 - \epsilon)\sigma_{\min}(\hat{\Sigma})]$ is stable. For Newton's method, define

$$g(\lambda) = \text{tr}(S_\lambda) - \kappa n, \quad g'(\lambda) = \sum_{j=1}^r \frac{\sigma_j}{(\sigma_j - \lambda)^2},$$

and update via $\lambda \leftarrow \lambda - \frac{g(\lambda)}{g'(\lambda)}$, projecting back into $(-\infty, (1 - \epsilon)\sigma_{\min}]$ to stay within the safe region.

Weighted Regularization $W \succeq 0$ For a general penalty $R(\theta) = \frac{1}{2}\theta^\top W\theta$, the trace becomes

$$\text{tr}(S_\lambda) = \sum_j \frac{\sigma_j}{\sigma_j - \lambda w_j},$$

so the same procedure applies with termwise substitutions $\sigma_j \leftarrow \sigma_j$, $\lambda \leftarrow \lambda w_j$ (from a generalized eigenvalue perspective).

D.2 Power-law Decay Schedule

While degree-of-freedom targeting can increase λ depending on the choice of κ (especially when r/n is small), we propose a more conservative alternative from a stability perspective: the *decreasing power-law schedule*:

$$|\lambda(n)| = |\lambda(n_0)| \left(\frac{n_0}{n}\right)^\alpha, \quad \alpha \geq 1.$$

Proposition 23 (Recommendation of $\alpha = 1$ via First-Order Balance). *From the optimism identity*

$$\mathbb{E}[\mathcal{R}(\hat{f}_\lambda)] = \mathbb{E}[\hat{\mathcal{R}}_S(\hat{f}_\lambda)] + \frac{2\tau^2}{n} \text{tr}(S_\lambda),$$

suppose for small λ that $\text{tr}(S_\lambda) = r + \lambda S_1 + O(\lambda^2)$, $S_1 = \sum_j \frac{1}{\sigma_j}$, and that $\hat{\mathcal{R}}_S(\hat{f}_\lambda) = \hat{\mathcal{R}}_S(\hat{f}_0) - B_1\lambda + O(\lambda^2)$ with $B_1 > 0$ representing the underfitting correction slope. Then the first-order term in test risk becomes

$$\Delta\mathbb{E}[\mathcal{R}] \approx -B_1\lambda + \frac{2\tau^2}{n} S_1 \lambda.$$

Balancing the two terms in order of magnitude suggests that $\lambda(n) \propto n^{-1}$ is a natural choice.

Heuristic. We compare the Taylor expansions of both terms and note that the variance penalty scales as $\frac{1}{n}$, so first-order balance yields $\lambda(n) = O(n^{-1})$. \square

Remark 9 (Practical Guidelines). *The default $\alpha = 1$ is recommended for general use. For noisier datasets or sharper spectra (many small σ_j), choosing $\alpha > 1$ leads to faster decay, mitigating instability near the safety boundary. Degree-of-freedom targeting and power schedules are alternative strategies: the former targets constant complexity, while the latter emphasizes conservative stability.*

D.3 Numerical Stabilization Notes

Safety Margin and Clipping Always enforce $\lambda \leq (1 - \epsilon)\sigma_{\min}(\hat{\Sigma})$, where $\epsilon \in [10^{-3}, 10^{-1}]$. For weighted regularization, use $\lambda \leq (1 - \epsilon) \min_j \frac{\sigma_j}{w_j}$.

Initialization Use the small- λ approximation $\lambda^{(0)} \approx \frac{\kappa n - r}{\sum_j 1/\sigma_j}$ as initial guess. If the value is negative, set $\lambda^{(0)} \leftarrow 0$. Spectral components can be approximated efficiently via randomized SVD or power iteration.

Line Search When using gradient descent or quasi-Newton methods, apply external line search to ensure descent in $\hat{F}_\lambda(\theta)$. After each step, project λ back into $(-\infty, (1 - \epsilon)\sigma_{\min}]$ to maintain the safety region.

Newton Damping In Newton updates $\lambda \leftarrow \lambda - \frac{g}{g'}$, multiply by a damping factor $\eta_\lambda \in (0, 1]$. If the new λ exceeds the safe region, iteratively halve η_λ until safety is restored.

Precision Management When $(\sigma_j - \lambda)$ becomes very small, numerical precision loss becomes critical. In such cases, either (i) reduce the target κ to push the root further away from the boundary, or (ii) cutoff small modes by excluding $\sigma_j < \delta$ from the trace approximation.

Log-Scale Tuning For practical hyperparameter tuning, perform one-dimensional search in $\log_{10} \lambda$ space (e.g., golden section). Combine this with boundary clipping for robust and efficient convergence.

E Spectral Weighting and Noise Direction Control

E.1 Smoother under Weighted Regularization

Let the regularizer be defined as $R(\theta) = \frac{1}{2}\theta^\top W\theta$, where $W \succeq 0$. The empirical objective becomes

$$\hat{F}_\lambda(\theta) = \frac{1}{n}\|y - X\theta\|_2^2 - \frac{\lambda}{2}\theta^\top W\theta,$$

and the normal equation is given by $(\hat{\Sigma} - \lambda W)\hat{\theta}_\lambda = \frac{1}{n}X^\top y$. Thus, the prediction $\hat{f}_\lambda = X\hat{\theta}_\lambda$ defines a linear smoother:

$$S_\lambda^{(W)} := \frac{1}{n}X(\hat{\Sigma} - \lambda W)^{-1}X^\top \in \mathbb{R}^{n \times n}, \quad \hat{f}_\lambda = S_\lambda^{(W)}y.$$

Safety Condition If $\hat{\Sigma} - \lambda W \succ 0$, then \hat{F}_λ is strongly convex and $\hat{\theta}_\lambda$ is uniquely defined. Let $\rho_{\max} = \rho_{\max}(\hat{\Sigma}, W)$ be the largest generalized eigenvalue of $\hat{\Sigma}v = \rho Wv$, then

$$\lambda < \frac{1}{\rho_{\max}(\hat{\Sigma}, W)} \iff \hat{\Sigma} - \lambda W \succ 0.$$

In particular, when $W = I$, this reduces to $\lambda < \sigma_{\min}(\hat{\Sigma})$.

Whitened Representation When $\hat{\Sigma} \succ 0$, let $A := \hat{\Sigma}^{-1/2}W\hat{\Sigma}^{-1/2} \succeq 0$, then:

$$S_\lambda^{(W)} = \frac{1}{n}X\hat{\Sigma}^{-1/2}(I - \lambda A)^{-1}\hat{\Sigma}^{-1/2}X^\top = \frac{1}{n}Z(I - \lambda A)^{-1}Z^\top, \quad Z := X\hat{\Sigma}^{-1/2},$$

with $Z^\top Z = nI$. This representation simplifies further derivations of degrees of freedom and variance.

E.2 Proof of Degrees of Freedom Formula

Proposition 24 (Degrees of Freedom under Weighted Regularization). *Under the above notation, let the eigenvalues of $A = \hat{\Sigma}^{-1/2}W\hat{\Sigma}^{-1/2}$ be a_1, \dots, a_r (where $r = \text{rank}(X)$). Then, for $\lambda < 1/\sigma_{\max}(A)$ (i.e., within the safety region),*

$$\text{tr}(S_\lambda^{(W)}) = \text{tr}((I - \lambda A)^{-1}) = \sum_{j=1}^r \frac{1}{1 - \lambda a_j}.$$

In particular, if $\hat{\Sigma}$ and W are simultaneously diagonalizable, i.e., $\hat{\Sigma} = U \text{diag}(\sigma_j)U^\top$, $W = U \text{diag}(w_j)U^\top$, then

$$\text{tr}(S_\lambda^{(W)}) = \sum_{j=1}^r \frac{\sigma_j}{\sigma_j - \lambda w_j}.$$

Proof. From the whitened representation,

$$\text{tr}(S_\lambda^{(W)}) = \frac{1}{n} \text{tr}(Z^\top Z(I - \lambda A)^{-1}) = \text{tr}((I - \lambda A)^{-1}) = \sum_j \frac{1}{1 - \lambda a_j}.$$

If $\hat{\Sigma}$ and W are simultaneously diagonalizable, then $A = U \text{diag}(w_j/\sigma_j)U^\top$, so that $\frac{1}{1 - \lambda a_j} = \frac{\sigma_j}{\sigma_j - \lambda w_j}$. \square

Remark 10 (Variance Term $\text{tr}((S_\lambda^{(W)})^2)$). A similar calculation yields:

$$\text{tr}((S_\lambda^{(W)})^2) = \text{tr}((I - \lambda A)^{-2}) = \sum_j \frac{1}{(1 - \lambda a_j)^2} \quad \left(\text{under simultaneous diagonalization: } \sum_j \frac{\sigma_j^2}{(\sigma_j - \lambda w_j)^2} \right),$$

showing that variance inflation in low-denominator directions is directly governed by the choice of weights w_j .

E.3 Design Principles for Spectral Weighting

Spectral weighting controls the *direction-specific amplification* of Anti-regularization. The key goal is to suppress over-amplification along directions with small singular or eigenvalues.

Principle 1: Maintain safety margin Always enforce the generalized safety condition $\lambda < 1/\sigma_{\max}(A)$. In practice, apply a margin:

$$\lambda \leq (1 - \epsilon) \frac{1}{\sigma_{\max}(A)} \quad (\epsilon \in [10^{-3}, 10^{-1}]).$$

Under simultaneous diagonalization, this becomes $\lambda \leq (1 - \epsilon) \min_j \sigma_j/w_j$.

Principle 2: Monotonic increasing weights To avoid excessive amplification in small- σ_j directions, set w_j as a *non-decreasing function* of σ_j . Typical designs include:

$$w_j = c \sigma_j^\beta \quad (\beta \geq 1, c > 0), \quad \text{or} \quad w_j = \min\{w_{\max}, c \sigma_j\}.$$

If $W = c \hat{\Sigma}$, then $A = cI$, yielding $\text{tr}(S_\lambda^{(W)}) = \frac{r}{1 - \lambda c}$, i.e., uniform amplification across all directions with minimal spectral distortion.

Principle 3: Degrees-of-freedom budgeting Target a desired per-sample complexity $\kappa > 0$ via

$$\frac{1}{n} \text{tr}(S_\lambda^{(W)}) = \kappa, \quad \text{or equivalently} \quad \sum_j \frac{1}{1 - \lambda a_j} = \kappa n.$$

Solve numerically, clipping $\lambda \leq (1 - \epsilon)/\sigma_{\max}(A)$ to prevent excessive sensitivity in small- a_j directions.

Principle 4: Suppress noisy directions To suppress amplification in directions known to be noisy or unstable, reduce w_j accordingly. For example, use leverage scores ℓ_j or cross-validation-based noise estimates $\widehat{\text{Var}}_j$:

$$w_j \propto \frac{\sigma_j}{\sigma_j + \tau_{\text{dir}}^2 \widehat{\text{Var}}_j}$$

so that larger noise implies smaller w_j , thereby suppressing $\frac{\sigma_j}{\sigma_j - \lambda w_j}$ expansion.

Principle 5: Hybrid schedule Combine spectral weighting with sample-size scaling:

$$\lambda(n) = \lambda(n_0) \left(\frac{n_0}{n} \right)^\alpha, \quad \alpha \geq 1,$$

while keeping W fixed or slowly adapting (e.g., via moving averages over w_j). This stabilizes $\text{tr}(S_\lambda^{(W)})/n$ over time.

Checklist

- (i) Estimate $\sigma_{\max}(A)$, then clip λ accordingly.
- (ii) Monitor $\text{tr}(S_\lambda^{(W)})$ and $\text{tr}((S_\lambda^{(W)})^2)$.
- (iii) Reduce w_j for small σ_j directions to mitigate amplification.
- (iv) Consider using $W = c\hat{\Sigma}$ as an approximation to improve A 's condition number.

F Classification: Lack of Lower Bound and Remedies

F.1 Constructive Examples of Unboundedness

We demonstrate that on *separable* data, the cross-entropy H with negative L_2 reward

$$\hat{F}_\lambda(\theta) = \frac{1}{n} \sum_{i=1}^n H(p_{y_i}, q_\theta(x_i)) - \frac{\lambda}{2} \|\theta\|_2^2, \quad \lambda > 0$$

can become *unbounded from below*.

Proposition 25 (Binary Logistic: No Lower Bound). *Let $y_i \in \{\pm 1\}$, logit $z_i(\theta) = \theta^\top x_i$, and loss $\ell_i(\theta) = \log(1 + \exp(-y_i z_i(\theta)))$. If the data is linearly separable, i.e., there exists $u \neq 0$ and $\delta > 0$ such that $y_i u^\top x_i \geq \delta$ for all i , then for the trajectory $\theta_t = tu$,*

$$\hat{F}_\lambda(\theta_t) \xrightarrow[t \rightarrow \infty]{} -\infty.$$

Proof. Each term satisfies $\ell_i(\theta_t) \leq \exp(-t\delta) \rightarrow 0$, while the reward term diverges as $-\frac{\lambda}{2} \|\theta_t\|^2 = -\frac{\lambda}{2} t^2 \|u\|^2 \rightarrow -\infty$. Thus, $\hat{F}_\lambda(\theta_t) \rightarrow -\infty$. \square

Proposition 26 (Multiclass Softmax: No Lower Bound). *For multiclass logits $f_\theta(x) \in \mathbb{R}^C$, define the correct-class margin $m_\theta(x_i, y_i) = f_\theta(x_i)_{y_i} - \max_{k \neq y_i} f_\theta(x_i)_k$. If there exists u and $\delta > 0$ such that $m_{tu}(x_i, y_i) \geq t\delta$ for all i , then*

$$\frac{1}{n} \sum_i H(p_{y_i}, q_{tu}(x_i)) \rightarrow 0, \quad \text{but} \quad -\frac{\lambda}{2} \|tu\|^2 \rightarrow -\infty,$$

and hence $\hat{F}_\lambda(tu) \rightarrow -\infty$.

Remark 11 (Interpretation). *Classification loss H can approach zero on separable data by scaling $\|\theta\|$ large, but the negative L_2 reward $-\frac{\lambda}{2} \|\theta\|^2$ diverges quadratically. Thus, negative L_2 regularization alone is insufficient to ensure stability in classification.*

F.2 Trust Region Remedy

Lemma 27 (Existence via Compactness). *Let $\Theta_B = \{\theta : \|\theta\| \leq B\}$ be a trust region of radius $B > 0$. Consider the constrained problem*

$$\min_{\theta \in \Theta_B} \hat{F}_\lambda(\theta).$$

If $H(\cdot)$ is continuous, then \hat{F}_λ is continuous on Θ_B , and by the Weierstrass theorem, a minimizer $\hat{\theta}_{\lambda, B}$ exists.

Proof. Θ_B is compact (closed and bounded subset of \mathbb{R}^p), and \hat{F}_λ is continuous. The Weierstrass theorem guarantees the existence of a minimum. \square

Remark 12 (Practical Guidelines). *The radius B may be chosen based on validation performance or numerical stability (e.g., logit saturation, gradient explosion). In practice, this is implemented via parameter clipping (e.g., $\|\theta\| > B \Rightarrow \theta \leftarrow B \theta / \|\theta\|$), or by weight normalization or norm constraints.*

F.3 Bounded Margin Reward ϕ

Instead of negative L_2 , we use a *bounded* margin reward ϕ to guarantee a lower bound.

Definition 1.

$$\hat{F}_\lambda^{(\phi)}(\theta) = \frac{1}{n} \sum_{i=1}^n H(p_{y_i}, q_\theta(x_i)) - \lambda \frac{1}{n} \sum_{i=1}^n \phi(m_\theta(x_i, y_i)),$$

where $\phi : \mathbb{R} \rightarrow [0, \phi_{\max}]$ is bounded and L_ϕ -Lipschitz.

Lemma 28 (Lower Bound Guarantee). *For all θ ,*

$$\hat{F}_\lambda^{(\phi)}(\theta) \geq -\lambda \phi_{\max}.$$

Hence, $\hat{F}_\lambda^{(\phi)}$ is bounded below.

Proof. Since $H \geq 0$ and $\phi \leq \phi_{\max}$, $\hat{F}_\lambda^{(\phi)}(\theta) \geq -\lambda \cdot \frac{1}{n} \sum_i \phi_{\max} = -\lambda \phi_{\max}$. \square

Remark 13 (Existence of Minimizer). *A lower bound does not guarantee the existence of a minimizer (e.g., when limit values are reached only at infinity). Thus, adding a trust region (see §F.2) or clipping logits/parameters (e.g., $|f_\theta(x)_k| \leq M$) to compactify level sets is advised. In practice, combining a bounded ϕ with parameter or logit clipping is recommended.*

Design Examples The following ϕ functions satisfy boundedness and Lipschitz conditions:

- (i) Capped Hinge: $\phi(m) = \min\{\max(m, 0), \phi_{\max}\}$, $L_\phi = 1$.
- (ii) Saturated Exponential: $\phi(m) = \phi_{\max} (1 - e^{-m/\gamma})_+$, $L_\phi = \phi_{\max}/\gamma$.
- (iii) Sigmoid Type: $\phi(m) = \phi_{\max} \sigma(m/\gamma)$, $L_\phi \leq \phi_{\max}/(4\gamma)$.

Stability (Gradient Bound) If the network is Lipschitz in parameters with constant G (i.e., $|m_\theta(x, y) - m_{\theta'}(x, y)| \leq G\|\theta - \theta'\|$), and ϕ is L_ϕ -Lipschitz, then

$$\left\| \nabla_\theta \frac{1}{n} \sum_i \phi(m_\theta(x_i, y_i)) \right\| \leq L_\phi G,$$

so the gradient norm of the reward term is bounded by $\lambda L_\phi G$, suppressing numerical explosions. Combining with *logit/gradient clipping* further enhances stability.

Practical Checklist (i) Calibrate ϕ_{\max}, γ on validation set (prevent over-rewarding large margins);
(ii) Combine logit clipping $f_\theta(x) \in [-M, M]^C$ and parameter clipping $\|\theta\| \leq B$;
(iii) Use sample-dependent scaling $\lambda(n) = \lambda(n_0)(n_0/n)^\alpha$, $\alpha \geq \frac{1}{2}$;
(iv) For non-separable data, use large γ to avoid early saturation of ϕ .

F.4 Generalization Bound Derivation

We present a generalization upper bound on 0–1 risk when using a bounded margin reward ϕ in classification. We adopt the same notation as in §F.3 and assume the following:

Assumptions (i) Either a trust region $\Theta_B = \{\theta : \|\theta\| \leq B\}$ or logit clipping $|f_\theta(x)_k| \leq M$ ensures compactness at the parameter/logit level.

(ii) The network is G -Lipschitz in parameters: $|m_\theta(x, y) - m_{\theta'}(x, y)| \leq G\|\theta - \theta'\|$.

(iii) The reward $\phi : \mathbb{R} \rightarrow [0, \phi_{\max}]$ is L_ϕ -Lipschitz.

(iv) A standard margin condition with margin width $\gamma > 0$ holds via ramp/hinge surrogate losses.

Theorem 29 (Combined Margin–Lipschitz Generalization Bound). *Under the above assumptions, for any $\delta \in (0, 1)$, with probability at least $1 - \delta$, the following holds for all $\theta \in \Theta_B$:*

$$\mathcal{R}_{0-1}(f_\theta) \leq \frac{1}{n} \sum_{i=1}^n H(p_{y_i}, q_\theta(x_i)) - \lambda \frac{1}{n} \sum_{i=1}^n \phi(m_\theta(x_i, y_i)) + C_1 \frac{G}{\gamma} \sqrt{\frac{1}{n}} + C_2 |\lambda| L_\phi \sqrt{\frac{1}{n}} + C_3 \sqrt{\frac{\log(1/\delta)}{n}}.$$

Here, $C_1, C_2, C_3 > 0$ are universal constants that may depend on the data radius or clipping constants.

Proof sketch. We outline the proof using the following steps:

(1) **Reduction to Margin.**

$$\mathcal{R}_{0-1}(f_\theta) = \mathbb{E}[\mathbf{1}\{m_\theta(x, y) \leq 0\}] \leq \mathbb{E}[L_\gamma(m_\theta(x, y))],$$

where L_γ is a ramp/hinge-type surrogate satisfying $\mathbf{1}\{m \leq 0\} \leq L_\gamma(m) \leq \mathbf{1}\{m \leq \gamma\}$.

(2) **Empirical–Expected Deviation (Rademacher/Contraction).**

Since $L_\gamma \circ m_\theta$ is (G/γ) -Lipschitz:

$$\mathbb{E}[L_\gamma(m_\theta)] \leq \frac{1}{n} \sum_{i=1}^n L_\gamma(m_\theta(x_i, y_i)) + C_1 \frac{G}{\gamma} \sqrt{\frac{1}{n}}.$$

(3) **Surrogate–CE Loss Comparison.**

Via standard calibration arguments, for some constant $c_0 \geq 0$:

$$\frac{1}{n} \sum_{i=1}^n L_\gamma(m_\theta(x_i, y_i)) \leq \frac{1}{n} \sum_{i=1}^n H(p_{y_i}, q_\theta(x_i)) + c_0.$$

(4) **Complexity of Reward Term.**

Since $\phi \circ m_\theta$ is $(L_\phi G)$ -Lipschitz:

$$\left| \frac{1}{n} \sum_{i=1}^n \phi(m_\theta(x_i, y_i)) - \mathbb{E}[\phi(m_\theta(x, y))] \right| \leq C_2 L_\phi G \sqrt{\frac{1}{n}}.$$

Hence, the $-\lambda \frac{1}{n} \sum \phi$ term contributes a correction of $+C_2 |\lambda| L_\phi \sqrt{1/n}$ to the bound.

(5) **Probability Boosting and Final Bound.**

Using McDiarmid's or Bernstein's inequality, we obtain with probability $1 - \delta$ an additional deviation term $C_3 \sqrt{\log(1/\delta)/n}$, yielding

$$\mathcal{R}_{0-1}(f_\theta) \leq \frac{1}{n} \sum_{i=1}^n H(p_{y_i}, q_\theta(x_i)) - \lambda \frac{1}{n} \sum_{i=1}^n \phi(m_\theta(x_i, y_i)) + C_1 \frac{G}{\gamma} \sqrt{\frac{1}{n}} + C_2 |\lambda| L_\phi \sqrt{\frac{1}{n}} + C_3 \sqrt{\frac{\log(1/\delta)}{n}}.$$

Constants C_1, C_2, C_3 are universal and may depend on the input norm bound or clipping radius. \square

Remark 14 (Interpretation). *The data-dependent terms in the bound consist of the empirical loss term $\frac{1}{n} \sum H - \lambda \frac{1}{n} \sum \phi$, while the complexity penalties separate into $O(\frac{G}{\gamma \sqrt{n}})$ and $O(|\lambda| L_\phi / \sqrt{n})$. Thus, to preserve generalization balance, $|\lambda|$ should decay at least as fast as $n^{-1/2}$.*

F.5 Proof of Sample-Size Scaling Rule

Theorem 30 (Sample-Size Scaling Rule in Classification). *Let $\lambda(n) = \lambda(n_0) \left(\frac{n_0}{n}\right)^\alpha$. If $\alpha \geq \frac{1}{2}$, then the complexity penalty in Theorem 29 remains bounded by $O(n^{-1/2})$. In particular, when $\alpha > \frac{1}{2}$, the reward-induced complexity term $C_2 |\lambda| L_\phi / \sqrt{n}$ decays faster, i.e., $o(n^{-1/2})$.*

Proof sketch. The reward-induced complexity term in the bound is $C_2 |\lambda| L_\phi / \sqrt{n}$. Since $|\lambda(n)| = \Theta(n^{-\alpha})$, the term becomes $\Theta(n^{-(\alpha+1/2)})$. To ensure it stays within $O(n^{-1/2})$, it is necessary and sufficient that $\alpha \geq 1/2$. If $\alpha > 1/2$, the decay becomes $o(n^{-1/2})$, implying a more conservative schedule. \square

Remark 15 (Practical Recommendation). *We recommend starting with the default value $\alpha = \frac{1}{2}$, and increasing α in settings with noisy data or small margin γ , where G/γ becomes large. This yields a more conservative decay for improved stability.*

F.6 Practical Notes on Stabilization

Logit and Gradient Clipping Clipping the logits as $|f_\theta(x)_k| \leq M$ and the gradients as $\|\nabla_\theta \ell\| \leq G_{\max}$ provides effective upper bounds on the Lipschitz constant, thereby reducing the complexity terms in generalization bounds.

Calibration of Margin Threshold γ Setting γ to the $q\%$ -th percentile (e.g., $q = 5 \sim 10$) of the margin distribution $m_\theta(x, y)$ on the training set prevents excessive penalties from the ramp/hinge surrogate, improving stability and calibration.

Combination with $|\lambda|$ Schedule Using a power schedule with $\alpha = \frac{1}{2}$ is a reasonable default. In early training stages when $|\lambda|$ is large, increasing the saturation threshold of ϕ (e.g., γ_ϕ in exponential-type designs) helps prevent premature reward saturation.

Compatibility with Trust Region Maintaining compactness of level sets—via either an explicit constraint $\|\theta\| \leq B$ or weight normalization—ensures the assumptions of Theorem 29 are stably satisfied throughout training.

Validation-based Early Stopping Monitoring both the validation objective $\frac{1}{n} \sum H - \lambda \frac{1}{n} \sum \phi$ and 0–1 accuracy helps detect unstable behaviors in early training. If over-rewarding causes excessive margin stretching for incorrect predictions, the schedule constant should be reduced immediately.

G Stability Perspective and the Need for Diminishing $|\lambda|$

G.1 Uniform Stability Bound

We analyze the uniform stability of the ERM solution or fixed point of a sufficiently converged first-order method under the following objective:

$$\hat{F}_\lambda(\theta) = \frac{1}{n} \sum_{i=1}^n \ell(\theta; z_i) - \lambda R(\theta),$$

where $\hat{\theta}_\lambda$ denotes the output model. The uniform stability is defined as:

$$\beta := \sup_z \sup_{i \in [n]} \left| \ell(\hat{\theta}_\lambda(S); z) - \ell(\hat{\theta}_\lambda(S^{(i)}); z) \right|,$$

with $S^{(i)}$ denoting the dataset S with the i th sample replaced by an independent copy.

Assumptions (i) Each loss $\ell(\cdot; z)$ is L -smooth and L_ℓ -Lipschitz in θ under trust-region or logit clipping constraints. (ii) The regularizer R is α_R -strongly convex. (iii) The empirical loss $\frac{1}{n} \sum_i \ell(\cdot; z_i)$ is μ -strongly convex. Then, the full objective is $\mu_{\text{eff}} = \mu - \lambda \alpha_R$ strongly convex, and the safe region is $\lambda < \mu/\alpha_R$ ensuring $\mu_{\text{eff}} > 0$.

Lemma 31 (Parameter shift from single data replacement). *Under assumptions (i)–(iii), we have*

$$\|\hat{\theta}_\lambda(S) - \hat{\theta}_\lambda(S^{(i)})\| \leq \frac{2G}{n\mu_{\text{eff}}},$$

where $G := \sup_{\theta, z} \|\nabla_\theta \ell(\theta; z)\|$ is a uniform gradient bound within the trust region.

Proof sketch. Subtracting the first-order optimality conditions for S and $S^{(i)}$, and applying the co-coercivity of μ_{eff} -strong convexity yields $\mu_{\text{eff}}\|\Delta\theta\| \leq \|\Delta g\|$. The gradient difference from a single sample change is $\|\Delta g\| \leq 2G/n$, which gives the result. \square

Theorem 32 (Uniform Stability Bound). *Under assumptions (i)–(iii), the uniform stability satisfies*

$$\beta \leq L_\ell \|\hat{\theta}_\lambda(S) - \hat{\theta}_\lambda(S^{(i)})\| \leq \frac{2L_\ell G}{n(\mu - \lambda\alpha_R)} = O\left(\frac{L_\ell}{n(\mu - \lambda\alpha_R)}\right).$$

In particular, the bound deteriorates as $\lambda \uparrow (\mu/\alpha_R)$, and vanishes as $\lambda \downarrow 0$ or $n \uparrow \infty$.

Remark 16 (Constant specification). *For squared loss with $\|x\| \leq R_x$, we obtain $G \leq R_x(\|X\theta\| + \|y\|)/n$. For cross-entropy with clipped logits $|f_\theta| \leq M$, a bound $G \leq M$ is obtained. In practice, the empirical maximum gradient norm on the validation set provides a reasonable estimate for G .*

G.2 Restoring $\beta \rightarrow 0$ via Scheduling

Proposition 33 (Stability under $|\lambda(n)|$ scheduling). *Suppose $\lambda(n) = \lambda(n_0) \left(\frac{n_0}{n}\right)^\alpha$. If the safety condition $\lambda(n) < \mu/\alpha_R$ is maintained, then the uniform stability satisfies*

$$\beta(n) \leq \frac{2L_\ell G}{n(\mu - \lambda(n)\alpha_R)} = \frac{2L_\ell G}{n\mu} \cdot \frac{1}{1 - \frac{\alpha_R}{\mu} \lambda(n)} \xrightarrow{n \rightarrow \infty} 0.$$

In particular, if $\alpha > 0$, then $\beta(n) = \frac{2L_\ell G}{n\mu}(1 + o(1))$, recovering the $O(1/n)$ rate of stability.

Remark 17 (Recommended α). *From a stability standpoint, any $\alpha > 0$ suffices. However, to balance other aspects discussed throughout the paper — such as the $|\lambda|/\sqrt{n}$ term in generalization bounds and degrees-of-freedom control in regression — we recommend $\alpha \geq 1$ for regression and $\alpha \geq \frac{1}{2}$ for classification.*

G.3 Checklist

Estimating the safety region Estimate μ and α_R , then enforce $\lambda \leq (1 - \epsilon)\mu/\alpha_R$. In regression, if $\mu = \sigma_{\min}(\hat{\Sigma})$ and $R(\theta) = \frac{1}{2}\|\theta\|^2$, then $\alpha_R = 1$.

Stepwise decay procedure Set an initial value λ_0 at sample size n_0 , and schedule $\lambda(n) = \lambda_0(n_0/n)^\alpha$. Recommended values are $\alpha \geq 1$ for regression and $\alpha \geq \frac{1}{2}$ for classification. The variable n may also refer to cumulative sample size under batch-wise or epoch-wise training.

Snapshot monitoring At each epoch, log the maximum gradient norm $\max_i \|\nabla \ell(\theta; z_i)\|$ and the effective strong convexity $\mu_{\text{eff}} = \mu - \lambda\alpha_R$, then monitor estimates of $\frac{L_\ell G}{n\mu_{\text{eff}}}$ accordingly.

Clipping and trust regions Apply logit/gradient clipping or a norm constraint $\|\theta\| \leq B$ to bound G and L_ℓ . This helps reduce the constants in Theorem 32.

Avoiding degeneracy If the effective curvature μ_{eff} falls below a threshold $\mu_{\min} = \eta_\mu \mu$, where $\eta_\mu \in [0.1, 0.5]$, then decay λ immediately or terminate training.

Weighted regularization $W \succeq 0$. If $R(\theta) = \frac{1}{2}\theta^\top W\theta$, then replace α_R with $\sigma_{\min}(W)$. The safety condition becomes $\lambda < \mu/\sigma_{\min}(W)$. If instability is observed along low-spectrum directions, increase the spectral mass of W to raise α_R .

G.4 Matrix calculus and auxiliary identities

This section collects frequently used identities and inequalities throughout the main text and appendix. Unless otherwise specified, all matrices are real symmetric, and $\|\cdot\|$ denotes the spectral norm.

Lemma 34 (Differentiation rules). *For an invertible matrix $M(\lambda)$, the following hold:*

$$\frac{\partial}{\partial \lambda} M^{-1} = -M^{-1} \left(\frac{\partial M}{\partial \lambda} \right) M^{-1}, \quad \frac{\partial}{\partial \lambda} \log \det M = \text{tr} \left(M^{-1} \frac{\partial M}{\partial \lambda} \right).$$

Also, for invertible A and constant B ,

$$\frac{\partial}{\partial \lambda} \text{tr}((A - \lambda B)^{-1}) = \text{tr}((A - \lambda B)^{-2} B).$$

Lemma 35 (Sherman–Morrison–Woodbury (SMW)). *For invertible A and appropriate shapes of U, C, V ,*

$$(A + UCV)^{-1} = A^{-1} - A^{-1}U(C^{-1} + VA^{-1}U)^{-1}VA^{-1}.$$

In particular, if $C = \alpha I$ and $V = U^\top$,

$$(A + \alpha UU^\top)^{-1} = A^{-1} - A^{-1}U(\alpha^{-1}I + U^\top A^{-1}U)^{-1}U^\top A^{-1}.$$

Lemma 36 (Spectral bounds). *For symmetric $A \succeq 0$ and any v ,*

$$\sigma_{\min}(A)\|v\|^2 \leq v^\top Av \leq \sigma_{\max}(A)\|v\|^2.$$

Also, if $\lambda < \sigma_{\min}(A)$, then

$$\|(A - \lambda I)^{-1}\| = \frac{1}{\sigma_{\min}(A) - \lambda}.$$

Lemma 37 (Weyl's inequality). *For symmetric matrices A and B ,*

$$\sigma_{\min}(A) + \sigma_{\min}(B) \leq \sigma_{\min}(A + B) \leq \sigma_{\max}(A + B) \leq \sigma_{\max}(A) + \sigma_{\max}(B).$$

Lemma 38 (Trace cyclicity and monotonicity). *For invertible A and any B , $\text{tr}(A^{-1}B) = \text{tr}(BA^{-1})$. If $0 \preceq B \preceq C$ and $M \succeq 0$, then $\text{tr}(MB) \leq \text{tr}(MC)$.*

Lemma 39 (Smootheness degrees of freedom derivative). *Given $\hat{\Sigma} = V \text{diag}(\sigma_j) V^\top$ and $\lambda < \sigma_{\min}(\hat{\Sigma})$,*

$$\text{tr}(X(X^\top X - n\lambda I)^{-1}X^\top) = \sum_j \frac{\sigma_j}{\sigma_j - \lambda}, \quad \frac{\partial}{\partial \lambda} \text{tr}(\cdot) = \sum_j \frac{\sigma_j}{(\sigma_j - \lambda)^2} > 0.$$

Remark 18 (Strong convexity and co-coercivity). *For a function F that is μ -strongly convex and L -smooth, the following hold:*

$$\langle \nabla F(\theta) - \nabla F(\theta'), \theta - \theta' \rangle \geq \mu \|\theta - \theta'\|^2,$$

$$\|\nabla F(\theta) - \nabla F(\theta')\| \leq L \|\theta - \theta'\|,$$

$$\langle \nabla F(\theta) - \nabla F(\theta'), \theta - \theta' \rangle \geq \frac{1}{L} \|\nabla F(\theta) - \nabla F(\theta')\|^2.$$

The combination of μ and L repeatedly appears in stability analysis.

G.5 Variants of Noise Assumptions

Heteroscedastic and correlated noise For general noise covariance $\Sigma_\varepsilon = \text{Cov}(\varepsilon) \succeq 0$, the optimism identity for a linear smoother $\hat{f} = Sy$ generalizes to

$$\mathbb{E}[\mathcal{R}(\hat{f})] = \mathbb{E}[\widehat{\mathcal{R}}_S(\hat{f})] + \frac{2}{n} \text{tr}(S \Sigma_\varepsilon).$$

When $\Sigma_\varepsilon = \tau^2 I$, this reduces to the classical form $\frac{2\tau^2}{n} \text{tr}(S)$. Under diagonal heteroscedasticity $\Sigma_\varepsilon = \text{diag}(\tau_i^2)$, the term becomes $\sum_i \tau_i^2 S_{ii}$, where higher leverage points contribute more to the variance term.

Sub-Gaussian noise If each ε_i is sub-Gaussian with parameter σ , the train–test gap still concentrates via Bernstein-type inequalities. With probability at least $1 - \delta$,

$$|\widehat{\mathcal{R}}_S(\hat{f}) - \mathbb{E}[\widehat{\mathcal{R}}_S(\hat{f})]| \leq C \sigma^2 \sqrt{\frac{\log(1/\delta)}{n}},$$

where the constant C may depend on $\|S\|_F$ or $\|S\| \text{tr}(S)$. Hence, the $\sqrt{\log(1/\delta)/n}$ term in the generalization bound of the main text remains valid in order.

Heavy-tailed noise When the sub-Gaussian assumption fails, using robust losses such as the Huber loss or median-of-means (MOM) regression approximately preserves the optimism identity. The deviation bound can still be restored to $\tilde{O}(\sqrt{1/n})$. In practice, one may estimate the contamination ratio q and set the Huber threshold κ to the corresponding quantile of the marginal distribution.

Weighted least squares and reweighting Under heteroscedasticity, weighted least squares with $W_\varepsilon \approx \Sigma_\varepsilon^{-1}$ yields the modified smoother

$$S = X(X^\top W_\varepsilon X - n\lambda I)^{-1} X^\top W_\varepsilon,$$

and the variance term in the optimism identity becomes

$$\frac{2}{n} \text{tr}(S \Sigma_\varepsilon) = \frac{2}{n} \text{tr}(X(X^\top W_\varepsilon X - n\lambda I)^{-1} X^\top),$$

under the approximation $W_\varepsilon \Sigma_\varepsilon \approx I$.

G.6 Counterexamples and Failure Cases

Deviating from recommended power schedules In regression, if the regularization strength $|\lambda(n)| \propto n^{-\alpha}$ is not followed and $\alpha < 0$ (i.e., $|\lambda| \uparrow$), the effective degrees of freedom $\text{tr}(S_\lambda)$ increase with n . As a result, the variance penalty in the optimism identity

$$\mathbb{E}[\mathcal{R}(\hat{f}_\lambda)] = \mathbb{E}[\widehat{\mathcal{R}}_S(\hat{f}_\lambda)] + \frac{2\tau^2}{n} \text{tr}(S_\lambda)$$

fails to vanish. In extreme cases where $\lambda \rightarrow \sigma_{\min}(\hat{\Sigma})$, both the degrees of freedom and numerical instability explode.

Failure in spectral weighting design Consider $\hat{\Sigma} = \text{diag}(1, \delta)$ for $0 < \delta \ll 1$, and set $W = \text{diag}(1, \delta^{-q})$ for $q > 0$. Then,

$$\text{tr}(S_\lambda^{(W)}) = \frac{1}{1 - \lambda} + \frac{\delta}{\delta^{1+q} - \lambda}.$$

The denominator in the low-variance direction becomes sharply small ($\delta^{1+q} - \lambda$), forcing an overly small admissible λ . Even slight changes in λ can cause wild fluctuations in the degrees of freedom. This illustrates a classic failure case where excessively large w_j are assigned to small σ_j directions.

Unbounded loss in classification For separable data, a negative L_2 penalty $-\frac{\lambda}{2}\|\theta\|^2$ leads to diverging loss: $H \rightarrow 0$ while $-\frac{\lambda}{2}t^2 \rightarrow -\infty$ along $\theta = tu$, hence $\hat{F}_\lambda \rightarrow -\infty$ (see Appendix F.1). Using only negative L_2 regularization in classification without trust region or bounded margin rewards is strongly discouraged.

Inconsistent initialization for DOF targeting To solve $\frac{1}{n} \text{tr}(S_\lambda) = \kappa$, the small- λ approximation

$$\lambda^{(0)} \approx \frac{\kappa n - r}{\sum_j 1/\sigma_j}$$

may yield negative values. Using such initial guesses can cause divergence in the root-finding process. In this case, it is safer to clip $\lambda^{(0)} \leftarrow 0$ and use bisection to find a unique solution.

Insufficient margin for stability From a stability perspective, if $\mu_{\text{eff}} = \mu - \lambda\alpha_R$ becomes too small, the bound $\beta = O(1/(n\mu_{\text{eff}}))$ worsens. In practice, it is recommended to enforce $\lambda \leq (1 - \epsilon)\mu/\alpha_R$, and to decay λ immediately once μ_{eff} drops below a predefined threshold.